2008-07-08

A Compliant Threshold Acceleration Sensor Integrated with Radio Frequency Identifiable Tags

Benjamin L. Todd
Brigham Young University - Provo

A COMPLIANT THRESHOLD ACCELERATION SENSOR INTEGRATED WITH RADIO FREQUENCY IDENTIFIABLE TAGS

by

Benjamin L. Todd

A thesis submitted to the faculty of

Brigham Young University

in partial fulfillment of the requirements for the degree of

Master of Science

Department of Mechanical Engineering

Brigham Young University

August 2008

BRIGHAM YOUNG UNIVERSITY

GRADUATE COMMITTEE APPROVAL

of a thesis submitted by

Benjamin L. Todd

This thesis has been read by each member of the following graduate committee and by majority vote has been found to be satisfactory.

Date	Brian D. Jensen, Chair
Date	Larry L. Howell
Date	Stephen M. Schultz

BRIGHAM YOUNG UNIVERSITY

As chair of the candidate's graduate committee, I have read the thesis of Benjamin L. Todd in its final form and have found that (1) its format, citations, and bibliographical style are consistent and acceptable and fulfill university and department style requirements; (2) its illustrative materials including figures, tables, and charts are in place; and (3) the final manuscript is satisfactory to the graduate committee and is ready for submission to the university library.

Date

Brian D. Jensen
Chair, Graduate Committee

Accepted for the Department

Matthew R. Jones
Graduate Coordinator

Accepted for the College

Alan R. Parkinson
Dean, Ira A. Fulton College of
Engineering and Technology

ABSTRACT

A COMPLIANT THRESHOLD ACCELERATION SENSOR INTEGRATED WITH RADIO FREQUENCY IDENTIFIABLE TAGS

Benjamin L. Todd

Department of Mechanical Engineering

Master of Science

Fully compliant bistable mechanisms have been proposed to be used as threshold accelerometers. The advantages to using these devices are that they require no external power to operate and maintain their sensing state. Using this characteristic the devices can be integrated with passive radio frequency identification tags (RFID). This allows for the sensing package to lay dormant with no maintenance needed until the sensor is read by the RFID reader. This thesis presents a successfully fabricated and integrated threshold accelerometer with a passive RFID tag. This in turn has been successfully read with an RFID reader and shown to act as a wireless passive sensor indicating whether or not a threshold acceleration has been exceeded. It is shown that in general plastics are not a suitable material to use in threshold accelerometers due to variability in fabrication, temperature and prolonged stresses inducing stress relaxation in the material. Multiple methods for testing the switching forces of these threshold accelerometers are developed and a frequency response for the switching forces of these devices is explored.

A straight-leg bistable mechanism design model is introduced and used to design metal bistable devices to reduce the variations seen in the plastic threshold accelerometers.

With this metal design a new fabrication process is introduced to attain thin metal compliant flexures with little variation in the thickness of the compliant flexures. This method allows for a more economical method of producing compliant flexures.

The metal bistable mechanism designs presented show significant improvement over the plastic bistable designs. These improvements include minimizing the effects of stress relaxation, minimizing variation in switching forces and minimizing variation between fabricated devices. The cost, however, with the metal bistable mechanism design would be more than the plastic bistable mechanism design.

ACKNOWLEDGMENTS

I'd like to thank my beautiful wife Afton for the many hours she has listened throughout this process. She has been a great help when the days were hard and tough. She has also been a great help in proofreading everything to get things just right. I would also like to thanks my kids Emma, Spencer and Peter for their bright and happy smiles and the shouts of joy when I arrive home that help remind me what is truly important in life.

My parents have been a great source of inspiration and strength throughout my life. I would like to thank them for all the learning opportunities they have provided for me in my life. They have been there giving advice and help in any way that they could, and I truly appreciate all that they have done for me.

Dr. Brian Jensen has been a great help also. He helped me talk out problems and look at things in a new light. I want to thank him for all the office visits, counsel and guidance. It has truly been a pleasure to work with someone who was so willing to take time out of a busy schedule to help teach and inspire me.

Dr. Larry Howell, Dr. Stephen Schultz and Dr. Aaron Hawkins have been there in countless meetings discussing data results and directing the research. Thank you for your input and help in everything.

I would also like to thank Kevin Cole, Ken Forster and the Precision Machining Laboratory for all their services, input and help in making this happen. Whether it was helping me set-up instrumentation, teaching me the best way to make parts, or simply providing services, your help has made this all possible.

Thank you to the faculty at Brigham Young University for the many classes taught and the examples of hard work and patience. I have had the chance to rub shoulders with some great people while here, and I will miss the chance to sit and learn from them in the classroom environment.

It has been a pleasure to be a part of the CMR lab. I would especially like to thank Kendall Teichert, Quentin Aten, and Garrit Larson for their camaraderie as well as their good input on problems. It has been a pleasure.

Finally, I am grateful to Heavenly Father in helping me with everything. He has truly answered prayers and provided inspiration in so many ways. There is no way this could have been done without him.

Table of Contents

List of Figures

Chapter 1

Introduction

There are currently many ways to sense data and report this data back to the user. In general, sensors need to sense whether an object has experienced a certain environmental input and report this back to the user in some way. Sensors do this by continuously monitoring and reporting the state back to the user through a wired connection or a wireless connection. The environmental input could take place anytime over an extended period of time. As such, the sensing device would have to be tied to a power source, such as a wall outlet or a battery pack as well as some kind of memory storage to remember the state of the sensed data. For example, a microphone uses the environmental input of pressure waves in air to record sounds. As seen in Figure 1.1 the microphone picks up the pressure waves and transmits these signals to a recording device, such as a computer. This recording device stores the data, which can then be used later to recreate the sounds or used to analyze the sound waves. The recording device requires some sort of power source in order to function properly. The microphone must be monitored continuously by the recording

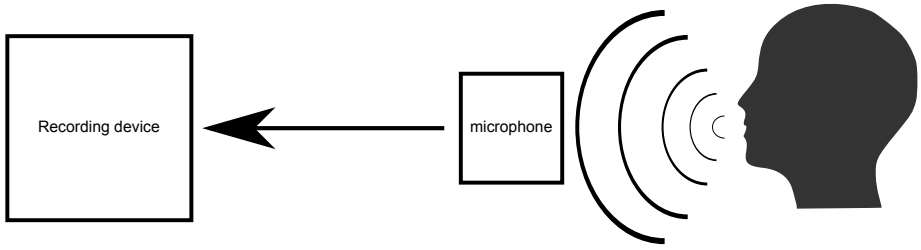

Figure 1.1: Diagram showing pressure waves, sensor device (microphone) and the memory device (recorder).

device in order to save the data. This works if the device could always be around a power source to prevent power loss and thus loss of data. In some cases a sensor is attached to a battery which provides the power remotely. However, if there is not a way to charge or replace the batteries in an environment, or a cost effective method to maintain the recorder, this would prevent the sensor from being placed within that environment. The objective of this research is to address this problem by combining a sensor with a radio frequency identification (RFID) tag. Specifically we will create a threshold acceleration sensor that is integrated with a passive RFID tag. The sensor's memory will be held in a sustained mechanical transformation of the sensor so that the sensor requires no power to sense the environmental input or to store the data. This transformation will be read by the passive RFID tag. An RFID reader would then be able to probe the RFID tag at anytime to determine whether or not the sensor has experienced an acceleration exceeding its switching threshold from the environment.

These sensors could be used in several areas of society. For example, the shipping industry currently has no way of determining where or when a fragile package was damaged. With this sensor integrated into the shipping company's tracking system, one could determine where the package was mishandled and/or potentially avoid a fraudulent claim that the shipping company was at fault. The sensors could also be placed in sensitive equipment such as hard drives and/or laptops. If the equipment was dropped and this drop caused the device damage in some form, the company could determine whether it was mistreated after the sale of the equipment or if the damage was caused by neglect of the consumer. The sensors could also be placed in a device such as an automobile. If a range of threshold sensors were placed in several locations in the automobile, an accident reconstruction of the events could be made with the data from the sensors. In turn this data could be used to determine who was at fault in an accident and potentially save insurance companies thousands of dollars.

Chapter 2 summarizes the background of compliant bistable mechanisms and how they work. Several specific versions of these devices are looked at, including fully compliant bistable mechanisms (FCBMs). RFID devices are also discussed including active and passive RFID tags as well as RFID sensors. Chapter 3 discusses some research done into

plastic FCBM's designed to act as threshold accelerometers. Switching forces for these devices will be measured and compared, as well as a discussion of the characterization of these accelerometers. A prototype of the RFID sensor is demonstrated and discussed. This chapter has been submitted as a research paper to the IEEE Sensors Journal. Chapter 4 discusses the variations seen in the plastic FCBMs and some reasons for these variations. It discusses material considerations in designing and results of these materials. Chapter 5 presents a metal design that reduces the variations seen in the plastic threshold accelerometers of Chapter 3. This design is compared to the plastic threshold accelerometers and advantages and disadvantages are discussed. Chapter 5 has also been prepared as a research paper for submission to the ASME Journal of Mechanisms and Robotics. Chapter 6 summarizes the findings and provides some recommendations for future work that could be done.

Chapter 2

Literature Review

Before going further in depth, some background is reviewed in the area of interest. First Radio Frequency Identification or RFID tags are addressed. This chapter discusses active and passive RFID tags as well as some sensors that have been developed using this technology. Compliant bistable mechanisms are discussed, including fully compliant bistable mechanisms.

2.1 Radio Frequency Identification (RFID)

Radio Frequency Identification or RFID tags are devices that use radio waves to transmit data from an identification tag back to a reader. The tag is made up of a microcontroller and an antenna. The tag is read by a reader sending out an electromagnetic wave as seen in Figure 2.1(a). The tag then responds to this electromagnetic wave as seen in Figure 2.1(b), and the reader interprets the data sent back by the tag. This is done by either inductive coupling using near field effects and/or far field effects. Most radio frequency or

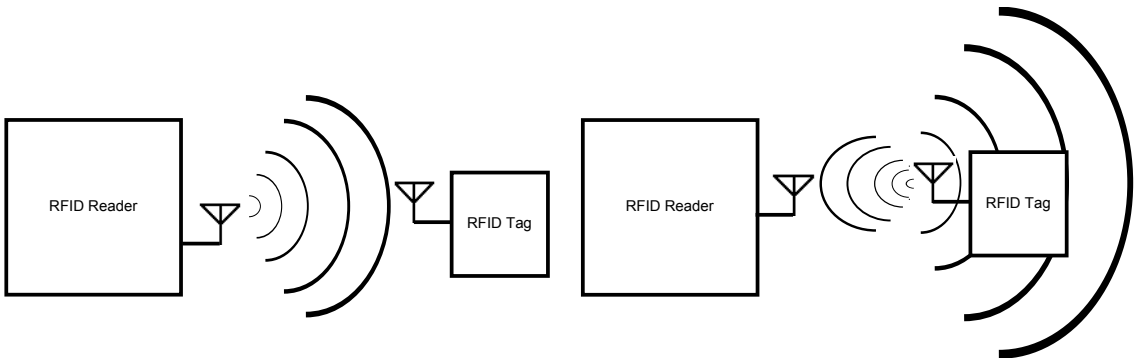

(a) An RFID reader querying an RFID tag. (b) An RFID tag responding to the readers query.

Figure 2.1: Basic function of an RFID system.

RF communication is performed using far field effects in other devices such as cell phones, radios or wireless internet connections. In general each tag has its own unique identification code that is sent back to the reader, allowing the reader to determine which tag it has read. Because of the possibility of multiple tags being in the reader's path, anti-collision methods are used to ensure that only one tag responds at a time, allowing the reader to not confuse the signal between tags. RFID tag's identification is stored in a non-volatile memory cell on board the chip. Currently there are many types of memory that can be obtained with varying capacities. Some types are: read-only memory where the memory is written during fabrication of the device and can not be changed; memory that can be written to only once and thereafter can only be read; and read-write memory where memory can be written multiple times, similar to a flash drive. Each of these types has its advantages and disadvantages depending on its application.

2.1.1 Active RFID Tags

Active RFID tags are tags that use some kind of on-board power supply to broadcast its identification code when a reader queries the tag. The power supply will allow the tag to respond with its identification with higher power and allow it to work in long range applications over 100 feet [1]. The power supply also allows the RFID tag to transmit its identification information multiple times to insure that the reader receives the information correctly. These devices are commonly used in areas where long read distances are needed or in "noisy" electromagnetic environments where it can be hard to read a signal from a tag. Active RFID tags are commonly used in express toll lanes so that the reader can be relatively far away and still receive the information from the tag. An example of this is seen in Figure 2.2. They are also commonly used in applications where the tag needs to record sensory data over long periods of time. However, these advantages come at a cost, namely that the tag package is large, the cost per tag is more than the other option of passive tags, and the battery must be maintained in order for the tag to respond when queried by the reader. It is estimated that a typical active RFID tag will last from 5-10 years [3] on a single battery.

Figure 2.2: An active RFID tag used in collection of highway tolls [2].

2.1.2 Passive RFID Tags

Passive RFID tags are tags that use only the energy from the reader's query signal to power its internal circuitry and respond back to the reader with its identification. This is done by using backscatter of the reader's electromagnetic signal when using inductive coupling. If inductive coupling is not used, a mini-transmitter is powered and sends the information using far field transmission techniques. Because there is no power supply with passive RFID tags, their range is limited. The range can be from a few centimeters to 29 meters [4] depending on the frequency used and the environment it is placed in. In general, the higher the frequency, the further the range of the tags, but, the further the read distance, the slower the data can be transfered. Since there is no on-board power supply, these passive tags also will have problems in "noisy" environments, and as such, the reader may have to be moved closer to the tag, or the reader will have to query the tag for identification several times. Some advantages of passive RFID tags are that they can be very small. This allows them to be placed in many locations without becoming a hindrance. The tag size is limited by the size of its antenna. Common antenna sizes used today range from 10 mm^2 to 1000 mm^2 [5], which can be seen in Figure 2.3. Further, passive RFID tags can be manufactured inexpensively. For example, researchers have developed a passive RFID tag that is projected to cost "pennies per tag" and can be read from 11 meters away [7]. Finally, passive RFID tags do not require any maintenance once they are placed. It is estimated that

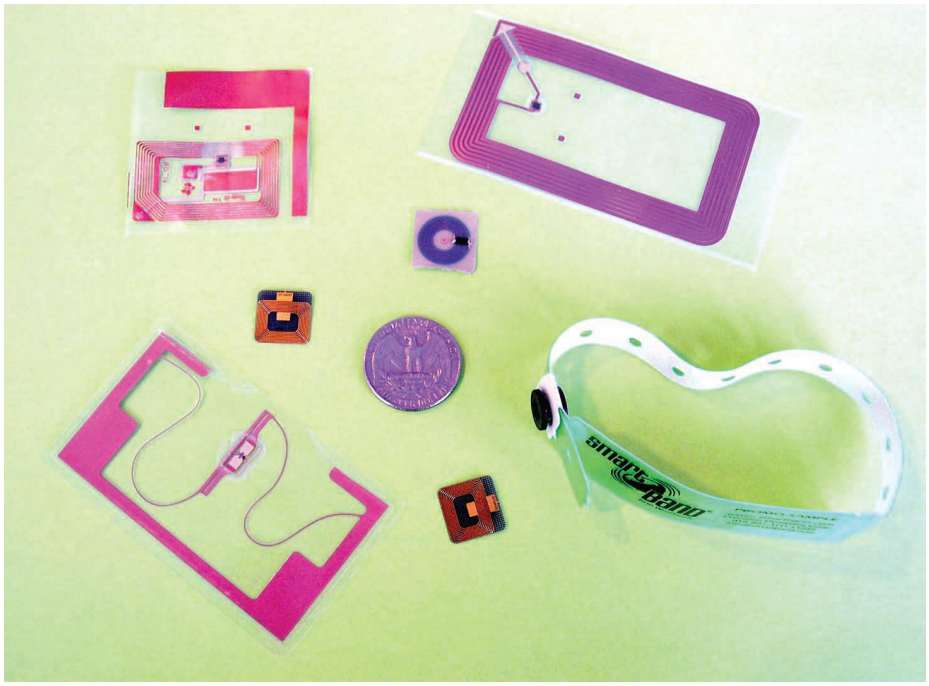

Figure 2.3: Passive RFID tags of varying sizes [6].

a passive RFID tag will essentially have an unlimited life span [3] and can be placed and forgotten until a reader queries the tag.

2.1.3 RFID Sensors

Due to the mobility and small size of passive RFID tags several sensor applications have been developed using this technology. Roy Want of Intel Research has said that RFID sensors must overcome two challenges:

> The sensor cannot use any power while the tag is not in communication with the reader, which is the usual operating state; and available energy is very small when the sensor is in reader range, which limits measurement techniques.

Roy goes on to give several examples of possible RFID sensors. These include a temperature sensor to determine if a temperature has exceeded some threshold, a product tamper sensor to determine if a product has been opened before delivery, sensors to determine if there has been exposure to harmful chemical, biological or radioactive agents, or acceler-

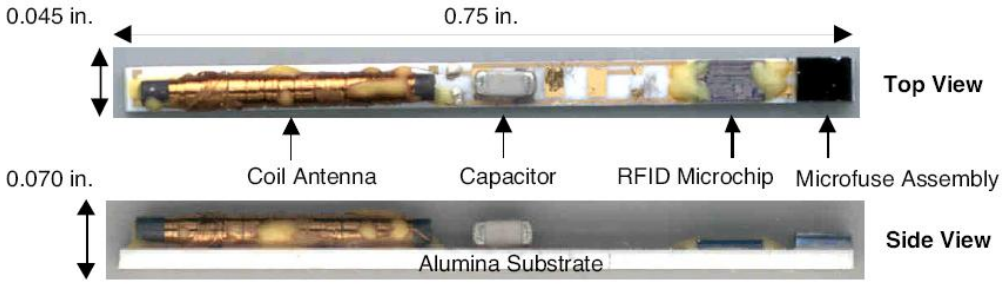

Figure 2.4: A passive RFID tag that uses a thermal fuse to determine if a temperature threshold has been exceeded [9].

ation sensors that measure a threshold impact or vibration input [6]. We will go more in depth on how some of these have been accomplished with some of the applications below.

Temperature sensors have been developed to be read via an RFID device. One type that has been envisioned is a threshold temperature sensor [8]. This sensor would have a device that changed impedance when a certain temperature was reached. This change in impedance could then be transmitted via the RFID tag back to the reader. Another RFID temperature sensor seen in Figure 2.4 that has been developed for NASA uses a thermal fuse. When a certain temperature is reached or exceeded, the fuse is destroyed and once again the tuned frequency changes, indicating to the reader that the temperature threshold has been exceeded [9]. Another temperature sensor that has been developed uses a proportional-to-absolute temperature current generator developed by Robert Widlar in 1965. Essentially this sensor takes the difference between two base-emitter voltages in transistors and uses the difference to determine the temperature. This sensor requires the reader to send a special code to the RFID tag that causes the tag's microprocessor to switch from its usual mode of using the harvested energy to send a signal back, to using the energy to read the state of the temperature circuit. This information is then stored in the RFID's non-volatile memory. The reader then queries the RFID tag again and gets the temperature information from the RFID tag's memory [10]. There are two examples of sensors that have been developed to determine whether they are in a wet environment [11] [12]. The first is done by having the inductor on the RFID tag exposed to the environment. This inductor is part of an LC tank circuit that is read by the reader through inductive coupling. The LC

circuit of the sensor is tuned to a specific frequency. When the inductor of the sensor is exposed to a wet environment, the impedance of the sensor's LC circuit changes. When the reader reads the state of the sensor, it gets a reading that is lower in voltage because of the slight offset in the tuned circuit caused by the impedance change. This gives the ability to wirelessly read the state of the sensor. The second type has a layer of carbon and zinc particles that are separated from a salt doped layer. When moisture is introduced between these layers, a battery is created. With the energy created from this battery, a transmission circuit is energized and transmits its identification code to a reader that is continuously monitoring the area.

A sensor to measure corrosion of rebar in concrete structures has been presented by researchers at Johns Hopkins University [13]. This sensor, seen in Figure 2.5, measures both temperature and conductivity to determine the state of the concrete around the rebar. The data can then be used to determine when repairs need to be made to the concrete structure. The device is powered by inductive coupling and is embedded into the concrete structure. The reader applies an electromagnetic signal to the device and once the circuity has reached a specified voltage, the sensors data is read into memory similar to the temperature sensor above [10]. The conductivity of the cement is measured using a transient resistance measurement. This is done by applying a constant current through the cement via two electrodes. The voltage is measured after a few milliseconds, and from this, the conductivity can be determined. The information is stored in memory as well. The reader then queries the RFID tag for the information.

Researchers at Intel and the University of Washington have developed a simple accelerometer that communicates via RFID tags [14], [11]. This sensor works by attaching a mercury switch to the antenna of an RFID tag. When the mercury in the switch completes the circuit, the RFID tag can be read. The switch is positioned to complete the circuit when at least a one-g load is experienced. Combining two RFID devices together with two mercury switches in opposite directions, as seen in Figure 2.6 will allow the user to determine which direction the sensor is placed because the reader will only "see" one of the tags at a time. Querying these RFID chips thousands of times in a second will allow

one to determine whether or not the sensor is experiencing a positive or negative g-force at certain times.

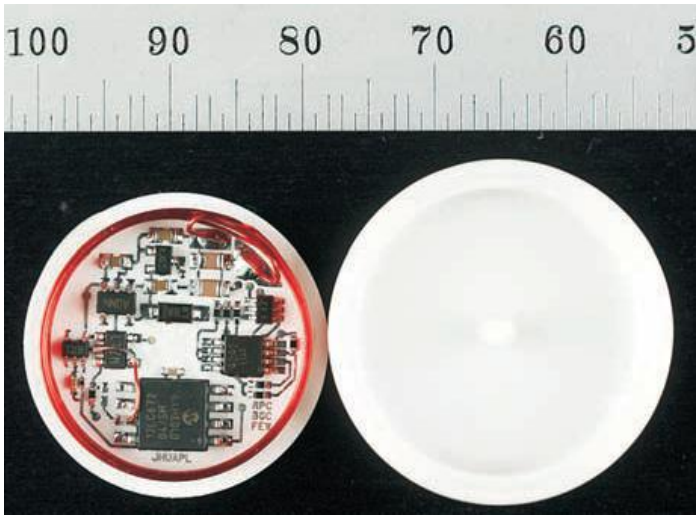

Figure 2.5: A passive RFID tag that is imbeded in concrete structures that measures temperature and conductivity to determine corrosion of internal rebar [13].

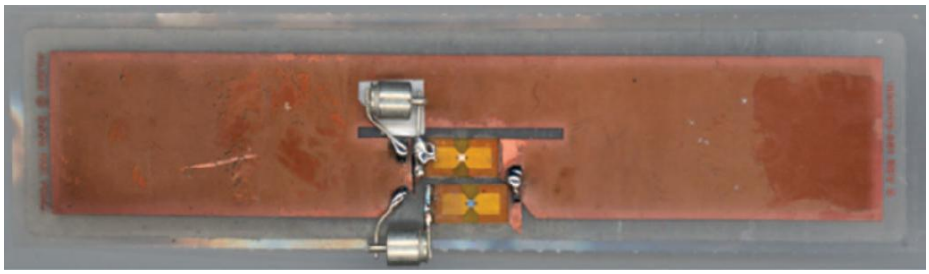

Figure 2.6: An accelerometer integrated with a passive RFID tag [14].

2.2 Compliant Bistable Mechanisms

Before describing compliant bistable mechanisms, some background in compliant mechanisms is needed. Compliant mechanisms are mechanisms where the structural members are allowed to flex or bend to allow for motion of the mechanism. As these members flex due to some external force, elastic energy is stored in the members. This can be used to the advantage of the designer. Several types of compliant mechanisms have been used

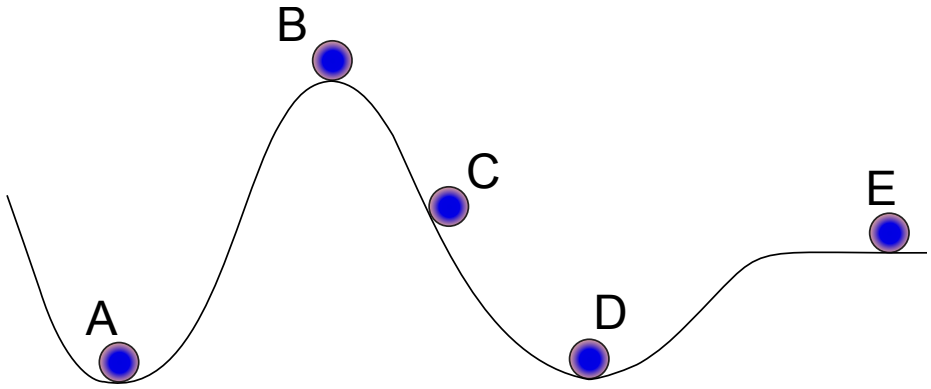

Figure 2.7: Ball on a hill analogy. Balls A,B,D and E are all in stable positions. Ball C is in an non-stable position. Balls A and D are in stable equilibrium. Ball B is in an unstable equilibrium position. Ball E is in a neutrally stable position.

throughout history, such as the catapult or bow and arrow. Today devices like paper clips or DVD/CD holders use compliant members to hold things into place. Ketchup and shampoo bottle caps use compliant members to hold a cap open or closed. Non-compliant mechanisms or rigid-body mechanisms can generally perform the same functions as compliant members. They usually use pin joints with a spring included in the joint, such as a stapler. When the stapler is depressed the spring is compressed and stores energy. When the stapler is released the head bounces back up to its lowest energy state. The advantage to compliant mechanisms is a reduction in part count leading to a decrease in assembly cost. There is also no friction and virtually no slop in the joint giving higher precision to the joint as well as longer life span to the product [15]. Rigid-body components can be used with compliant body components. However, if all the motion in a mechanism is obtained from compliant members, then it is categorized as a fully compliant mechanism.

2.2.1 Bistable Mechanisms

Bistable mechanisms are mechanisms that have two stable positions. The most familiar mechanism is that of a light switch. It will remain in its on or off position without any outside input to the mechanism. If a force is exerted onto a switch in the on position it could move to the off position, as long as that force exceeds a certain threshold. The best way to understand bistable mechanisms is using an analogy of a ball in a hilly environment seen in Figure 2.7. Balls A and D are said to be in stable equilibrium positions. This would

be like the on and off positions of the light switch. If there is some force put on these balls they will move up the hill, but if the force is removed they will settle back into their stable positions. Ball B is said to be in an unstable equilibrium position. The ball will balance on the top of the hill, but any force exerted on the ball in either direction will cause the ball to drop and settle to position A or D. Ball C is in an unstable position and cannot remain in that position. Ball E is said to be in a neutrally stable position. If the ball has some force exerted on it, it will move to a new position but stay in that position when the force is removed, unless it reaches the hill portion.

Another way to look at this is in terms of the potential energy of the balls. If the potential energy is at a local maximum then it would be an unstable equilibrium. If the potential energy is at local minimum then it will be a stable equilibrium position. If there is no change in potential energy in either direction then it would be a neutrally stable position.

Many configurations have been characterized and developed that are bistable [16]. These devices have been rigid-body mechanisms, partially-compliant mechanisms and fully-compliant mechanisms. In the next sections we will cover a few of these devices.

2.2.2 Early Bistable Devices

One of the early bistable mechanisms designed was the Young mechanism by B. Jensen [17]. This mechanism is defined by three conditions.

- The mechanism has two revolute joints, and, therefore, two links, where a link is defined as the continuum between two rigid-body joints.
- The mechanism has two compliant segments, both part of the same link.
- The mechanism has a pseudo-rigid-body model which resembles a four-bar mechanism.

These attributes can be seen in Figure 2.8. This bistable device is a partially-compliant mechanism and was designed with MEMS scales in mind. There are some disadvantages to this design. One of the largest of these is the pin joints. Slop in the pin joints causes the device to have backlash. It also allows wear in the device, and thus allows the switching force to possibly change over time. Fabricating these devices requires multiple layers,

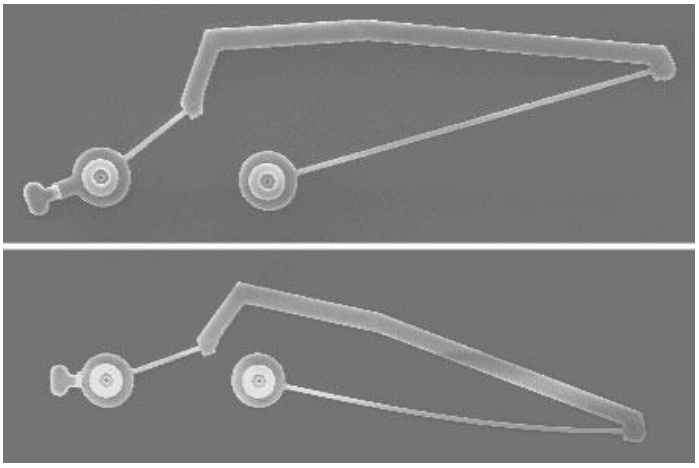

Figure 2.8: A bistable Young mechanism in its first(manufactured) and second stable positions [17].

increasing the complexity of the fabrication process and design. Another drawback to this design is that the input force required to change the device from one stable position to the other does not act in a straight line, meaning the force vector will have to change directions with the device in order to cause it to change its stable positions. This is not wanted in sensor applications where acceleration being measured acts in one direction.

Another bistable device created is the linear displacement micromechanism [18]. This is another partially-compliant mechanism that has linear movement between stable positions. The advantage to this device is that the input force to move the device from its first stable position to its second stable position will act in a straight line with no moments involved. It has several pin joints as seen in Figure 2.9, so it will have some of the same drawbacks as the Young mechanism mentioned earlier. This mechanism will stay in the first stable position until it is displaced to the point that the pin joints are parallel with each other. This correlates to position B in Figure 2.7, or the unstable equilibrium point. Any movement in the direction of motion of the device will cause it to move to either the first or second stable positions.

2.2.3 Fully Compliant Bistable Mechanisms

The fully compliant bistable mechanism or FCBM is similar to the bistable linear displacement micromechanism [19, 20]. This device is fully compliant, meaning it does not have any pin joints in the mechanism, as can be seen in Figure 2.10. Advantages of

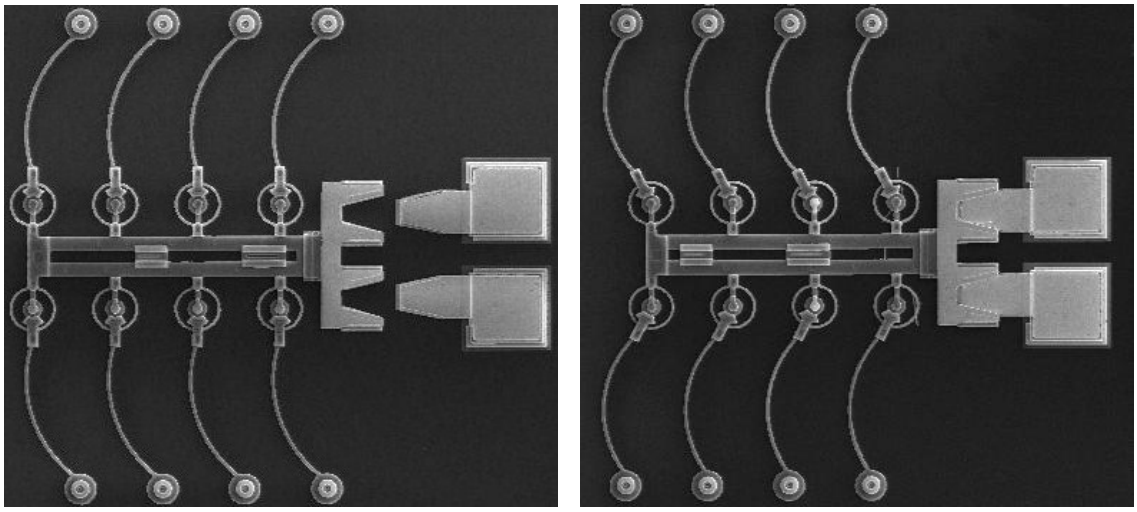

(a) Mechanism in the fabricated 1st stable position. (b) Mechanism in the 2nd stable position.

Figure 2.9: A bistable linear displacement micromechanism.

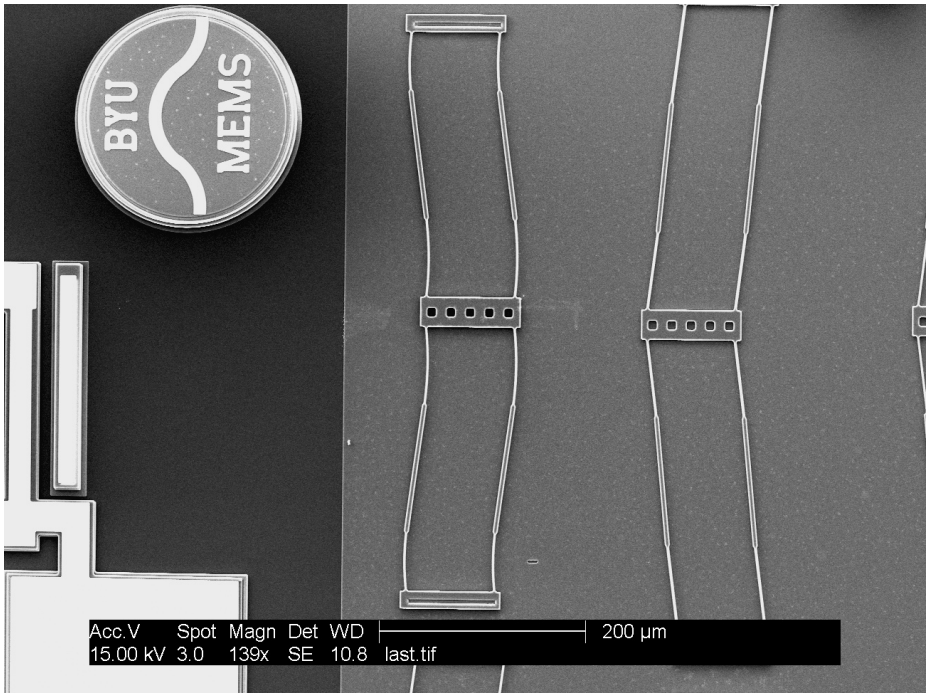

Figure 2.10: A fully-compliant bistable mechanism in its first and second stable positions.

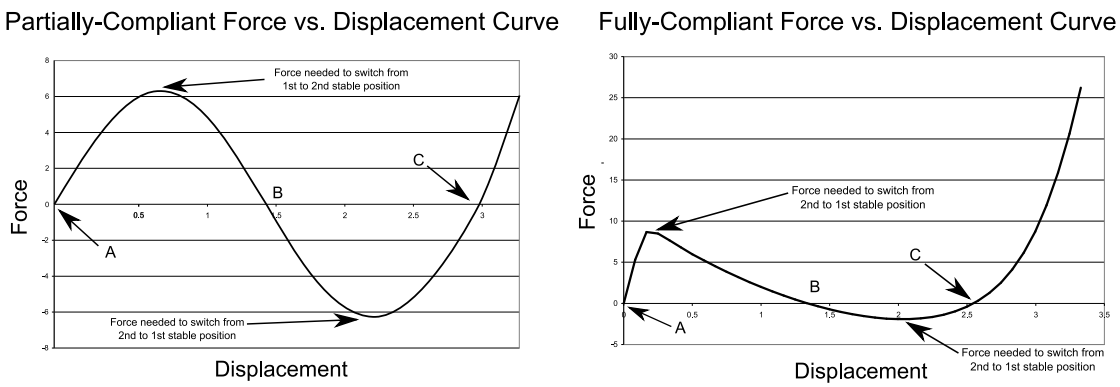

Figure 2.11: Force vs. displacement curves for Partially and Fully compliant bistable mechanisms. Point A is the first stable position, point B is the unstable equilibrium position and point C is the second stable position.

these devices are no backlash, friction or wear because there are no pin joints. Another property of this device is the force needed to actuate it from the first stable position to the second stable position and from the second stable position to the first stable position are not the same. In the linear displacement mechanism the forces needed to switch the device between its first and second stable and its second and first stable positions were equal as can be seen in Figure 2.11. The difference in switching forces can be used to our advantage and will be discussed later on. Motion in the device is achieved by inputting a force on the center shuttle. As the shuttle is displaced the four compliant legs will deflect and excert a force either in the forward or backward direction, depending on where it is on the force versus displacement curve in Figure 2.11. If the displacement exceeds the unstable equilibrium then the force becomes negative and the device's legs push the center shuttle into its second stable position. If the displacement does not exceed the unstable equilibrium the force becomes positive and the device's legs pull the center shuttle back into the first stable position.

Chapter 3

Low Cost RFID Shock Sensors

3.1 Abstract

[1]This paper describes a battery-free threshold shock sensor with wireless readout via RFID circuitry. The entire package is designed to provide low-cost sensors for monitoring shock loads in applications such as shipping. The sensor is based on a mechanical bistable mechanism laser-cut from a single Delrin layer which switches states when exposed to accelerations above a threshold. The sensor was tested using quasi-static accelerations in a centrifuge, pulsed accelerations from an impact event, and vibration (sinusoidal) accelerations on a shaker table. Measured threshold accelerations were similar in magnitude for the three load types, although they varied slightly due to dynamic effects. This phenomenon was further explored using a dynamic model of the sensor. Threshold accelerations in the range of 30 to 50 G's were measured, and these values can be varied by changing the mass of the accelerometer's outer frame. Wireless readout was successfully demonstrated by using the mechanical accelerometer as an electrical switch connected to the sensor input of an RFID chip.

3.2 Introduction

Threshold shock sensors, also called latching accelerometers, record an acceleration event above a specific threshold. These sensors are typically designed for long-term monitoring. An example application arises in the shipping industry in which shock events invariably occur but are difficult for customers to monitor. For instance, a study found that

[1]This Chapter is a paper submitted to IEEE Sensors Journal and was co-authored by Mallory Phillips, Stephen M. Schultz, Aaron R. Hawkins, and Brian D. Jensen

a package sent second-day air would on average experience a drop from a height of 1-1.85 m during transit [21]. Another study showed that an average commercial truck would induce G-loads from 5-35 G's [22]. A sensor could be mounted on a shipping container to determine if a shock beyond a threshold value had been experienced in the transit of the container. Ideally, shock sensors would require zero electrical power, be small in size, and be low cost. Additionally, they should be easy to monitor and deployable in a network — for instance, multiple sensors attached to packages inside a shipping truck. One example of a shock sensor currently used in shipping is a product called ShockWatch®, which employs a small tube filled with a dye. When a package experiences a certain level of shock [23] a seal in the tube is broken and it changes color. ShockWatch® sensors cost around $2 per device and can only be read by visual inspection. This sensor requires zero electrical power and is relatively small in size, but its manual readout mechanism does not lend itself easily to a high-speed monitoring or networks. This paper introduces a shock sensor design that requires zero power, is small, low cost, and can be remotely monitored. The sensor combines a latching accelerometer with a Radio Frequency Identification (RFID) chip. The accelerometer is a mechanical element that changes states when a threshold acceleration is met. The element's state can be relayed wirelessly to an electronic reader via the RFID chip. Multiple RFID chips can be read simultaneously, making sensor networks possible.

RFID technology has seen rapid development and deployment in the last several years due to its potential to dramatically improve inventory control in retail and military distribution networks [24]. In RFID systems, a reader sends out a radio frequency signal. Passive RFID chips receive this signal through an attached antenna; they use the radiation in the signal to power an on-board microcontroller. The microcontroller encodes data stored in the chip's memory into a return signal that is reflected back to the reader. In this way, the chip is identified, and the package it is attached to is tracked through a supply chain. RFID chips are programmed to use an effective anti-collision algorithm to allow the reader to communicate reliably with many chips at the same time. The read distance for passive RFID chips is up to 10 m [25], [26], with some examples of an even higher range. Existing RFID chips are also inexpensive (less than $0.50 each is typical), and the read rate is reasonably high at about 2,000 reads per second [14]. Identification of individual sensors is

also easy, since each RFID chip is already programmed with a unique electronic signature. There are several previously reported examples of RFID-based sensors, demonstrating that the technology is feasible and adaptable. Researchers at Intel and the University of Washington have demonstrated a simple accelerometer that communicates via RFID [14], [11]. A sensor to detect pathogens in food has also been proposed [8]. A sensor to measure corrosion of rebar in concrete structures has been presented by researchers at Johns Hopkins University [13] and a group at the University of Georgia has also demonstrated a temperature sensor that communicates via RFID [27]. This paper presents the design concept for a mechanical shock sensing element and how it can be electrically connected to an RFID chip. The resulting sensor remotely communicates the position of the mechanical element after an acceleration event. Test results are shown in response to several stimuli: constant acceleration provided by a centrifuge, a short acceleration pulse due to impact, and oscillating acceleration due to vibration.

3.3 Sensor Concept

The mechanical element in the new shock sensor uses a bistable mechanism that is fully compliant [28]. As Figure 3.1 shows, this device consists of a center shuttle that is actuated with some input force. Flexible segments are attached to the center shuttle to allow motion. As a force is applied on the center shuttle of the device the flexible legs will deflect and eventually reach a state in which the device will pull itself into a second stable position. Figure 3.2 shows the force on the center shuttle versus its displacement. There

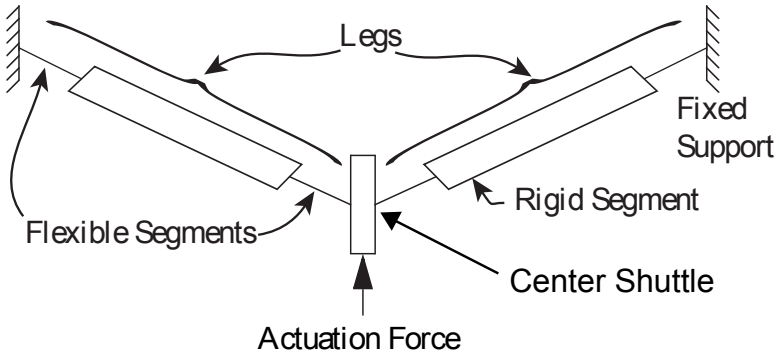

Figure 3.1: Mechanical schematic of the compliant bistable mechanism. The flexible segments allow for motion into two stable positions.

are three displacements where the reactive force is zero. Point A is the fabricated position of the device and is the first stable position. Point C is the second stable position and point B is the unstable position. If the device were placed in this unstable position a slight force in either direction would move the device into the first or second stable position, depending on the direction of the force.

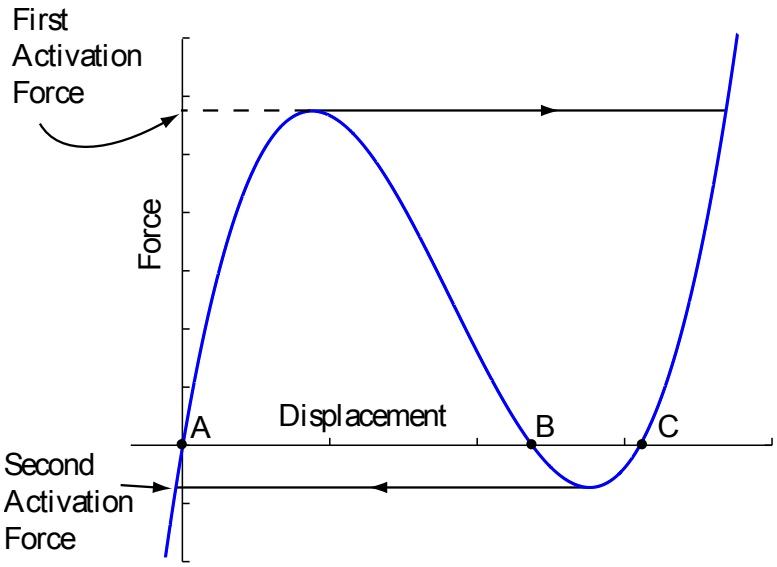

Figure 3.2: Representation of the force vs. position for the central shuttle of the bistable mechanism shown in Figure 3.1. Position A and C are the stable positions. Position B represents the unstable position.

To move the device out of the first stable position, or point A, a force that is greater than the first activation force in Figure 3.2 is needed. If this force is reached the device will move to the second stable position at point C. Similarly, if the device is in the second stable position it would need a force with magnitude larger than the second activation force in Figure 3.2 to switch. This force would cause the device to move to the first stable position at point A. In our application, we will preset the device to the second stable position. If a shock is sensed that creates an inertial force larger than the second activation force, the device will switch to the first stable position. Since the magnitudes of the first and second activation forces are 5-10 times different, the device will tend to stay in the first stable position at point A. This effectively keeps the device latched into the first stable position after a threshold acceleration is sensed. To determine the acceleration required to achieve

the desired switching force we use the equation

$$F = ma \tag{3.1}$$

where F is the force, m is the mass of the center shuttle of the device and a is the acceleration experienced. In our case we have created a kinematic inversion of the device so that the center shuttle is anchored and the outer frames mass is used. This allows the acceleration needed to switch the device to be easily changed by adding or taking away the mass from the frame of the device. In this way, one could calibrate the device to switch at any of many desired accelerations. Because this device retains its state over time, it can be used as a memory element without the need for electrical power. In order to electrically integrate the mechanism with an RFID chip, its motion from the second to first mechanical state will close electrical contacts. This switch will change a resistive load across two input nodes for the RFID chip. As can be seen in Figure 3.3, the complete sensor package only requires space for the mechanical element, the RFID chip, the electrical contacts, and the inductive antenna.

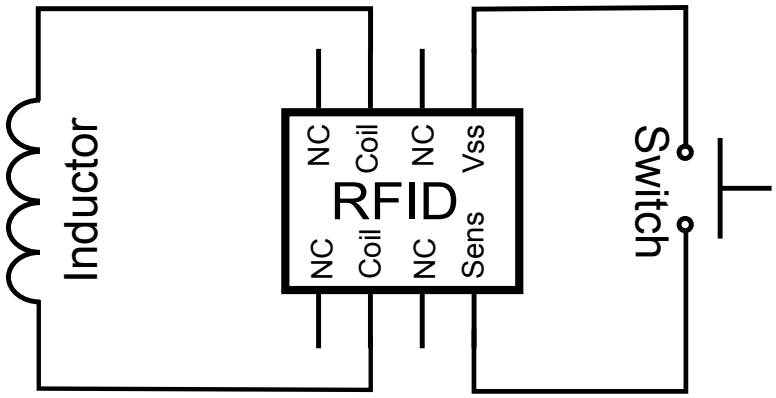

Figure 3.3: Electrical schematic showing components used in the sensor prototype.

3.4 Sensor Prototyping

The bistable accelerometer can be made from a single material layer. This is attractive because manufacturing costs are lower than when multiple layers are required. To

demonstrate one low-cost manufacturing method, accelerometers were formed by cutting a plastic sheet with a commercially available laser cutter. The specific plastic used was Delrin because it proved to have especially good stiffness and laser cutting properties compatible with our device designs [29]. A Universal Laser Systems (Scottsdale, Arizona) C-200, which uses a CO_2 laser with a cutting width of around 200 micrometers and a power of 25 W, performed the cutting. Cutting speeds ranged from 20 mm/s to 67 mm/s, resulting in cutting times for devices between 9.2 to 20 seconds. It was found to be preferable to make cuts with two or three passes, depending on plastic thickness. Attempting to cut with a single pass could overheat the plastic, causing extreme warping. Creating compliant mechanism designs in plastic could potentially be done with other plastic formation or machining techniques. Figure 3.4 shows a Delrin sensor fabricated by laser cutting. A typical sensor had outer dimensions of 28 mm by 26 mm, making the area of the outer portion of the sensor about 900 mm^2.

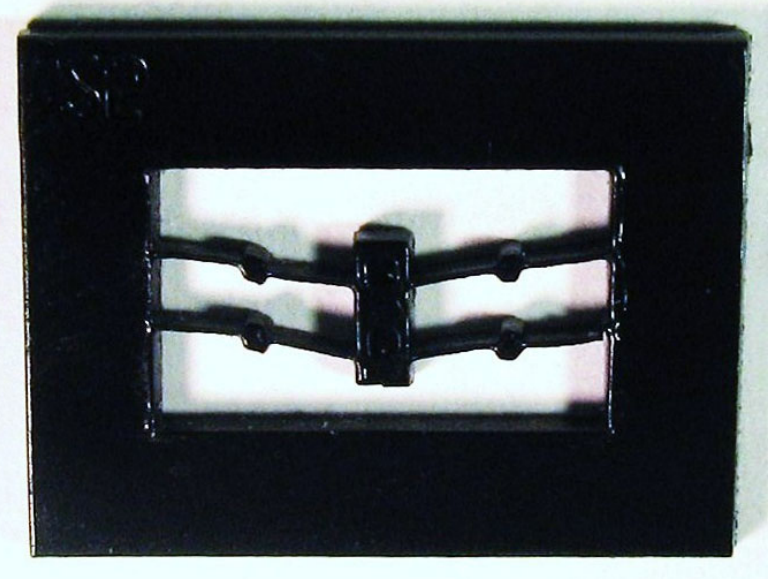

Figure 3.4: Bistable mechanism fabricated by laser cutting of Delrin.

The accelerometer design included two square holes cut into the center piece of the compliant mechanism. The holes functioned as a fit for two pins that would anchor the compliant mechanism in place on a printed circuit board (PCB). This system of sliding the compliant mechanism onto pins proved very efficient when many sensors needed to be

tested. Upon testing a number of bistable accelerometers, it was observed that there was some variation in their threshold acceleration even when they had the same frame mass. It was determined that this variation was due to inexact laser cutting. As seen in Figure 3.4, when creating the thin lines used for the legs of the bistable accelerometer, the plastic tends to melt and bead up. This beading is somewhat random and causes the thickness of the compliant leg members to vary throughout the leg, resulting in a variation in switching thresholds. We measured the device-to- device variation to be 10.4% for devices of the same mass.

A concept CAD drawing of the sensor is shown in Figure 3.5. To complete the sensor, a PCB was fabricated and a RFID tag was integrated with the plastic accelerometer as seen in Figure 3.6. Adhesive-backed aluminum strips were placed on one side of the accelerometer's outer frame so that when it changed positions it would close an electrical switch by completing the connection between two pins inserted into the PCB. For the RFID chip, we used model ATA5570 from Atmel (San Jose, CA). This is a passive chip with read/write data transmission operating at a frequency of 125 kHz. It comes in an 8-pin SO8 package and requires an external antenna for communication and power. This chip was chosen primarily because it has a built-in sensor input. The chip's output data stream inverts when a resistor less than 100 kohms is connected between this sensor input and ground. The circuit diagram in Figure 3.3 shows the connections between the chip and accelerometer, as well as the necessary components for the chips RF antenna.

An evaluation module available from Atmel (ATA2270-EK1) was used to read and write to the RFID chip. The module had a working distance of 3 cm, although it can be modified by adding a preamplifier to give it a working distance of 10 cm. Passive RFID chips are available that operate at higher frequencies and have larger working distances. We are not aware, however, of a current high- frequency/high-working-distance chip that has a sensor input.

3.5 Sensor Characterization

Three methods were used to measure the switching acceleration, in G's, needed to flip the sensor from its second to its first stable position. This was done to verify that the

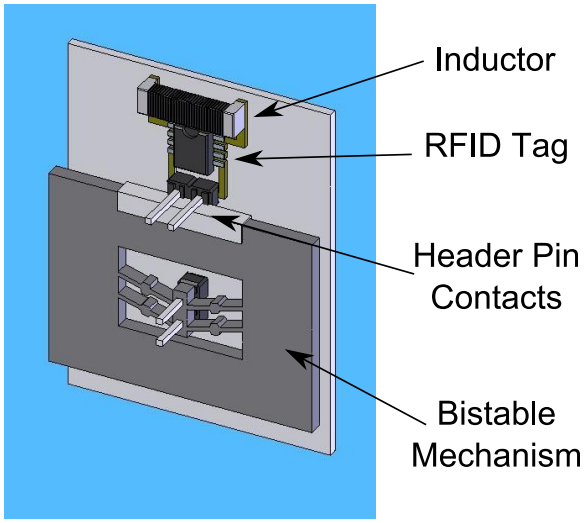

Figure 3.5: A concept CAD drawing of a shock sensor showing the inductor, header pin contacts and RFID chip with the sensor.

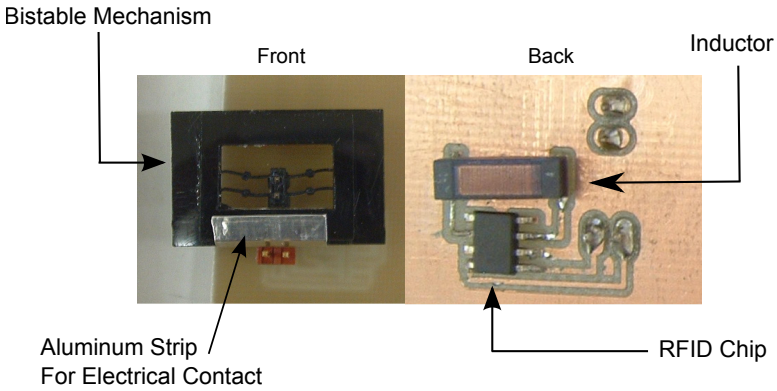

Figure 3.6: A working shock sensor prototype, front and back view showing the inductor and RFID chip with the sensor.

switches would perform under varying load conditions. The first testing method, shown in Figure 3.7, applied a constant acceleration using a centrifuge, specifically a Model K, manufactured by International Equipments Company (Needham, Massachusetts). The acceleration can be calculated from the speed of the centrifuge using the equation

$$a = R((2\pi\omega)/(60))^2 \tag{3.2}$$

where a is the acceleration in m/s^2, R is the radius of rotation in meters, and ω is the angular velocity of the centrifuge in rpm. The radial distance of the sensor from the centrifuge's

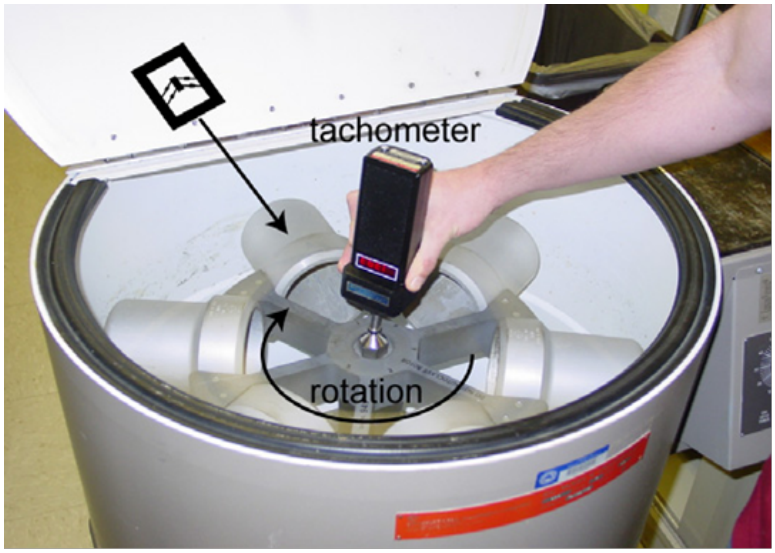

Figure 3.7: The centrifuge test showing the tachometer and centrifuge.

center was $R = 0.2431$ m and the centrifuge had a maximum angular velocity of around 1800 rpm, resulting in an acceleration range between 0 and 881 G's.

The second test method applied impact acceleration to the sensor using a drop tester. The drop tester was designed and built in steel specifically for these sensors. Padding was placed on the flat striking surface to vary the impact pulse width. A layer of neoprene and a thin piece of rubber were ultimately used for padding, resulting in a pulse width of approximately 5 ms. A shuttle was used to anchor the sensor with a PCB Piezotronics model 303A accelerometer attached as seen in Figure 3.8. A one-meter rod was used to guide the shuttle to the striking surface. The Piezotronics accelerometer was integrated with LabVIEW to take acceleration measurements. A typical acceleration pulse is seen in Figure 3.9. Acceleration magnitude could be varied by dropping the shuttle from different heights.

The third test method used was a shaker table to apply vibrations to the sensor. Using a similar setup to the drop tester, the sensor and Piezotronics accelerometer were attached to an anchoring bar and placed inside a MB Electronics PM-50 Model shaker table. A sinusoidal voltage at 100 Hz was applied to the shaker table and accelerations were measured using the commercial accelerometer and the LabVIEW software. A fast

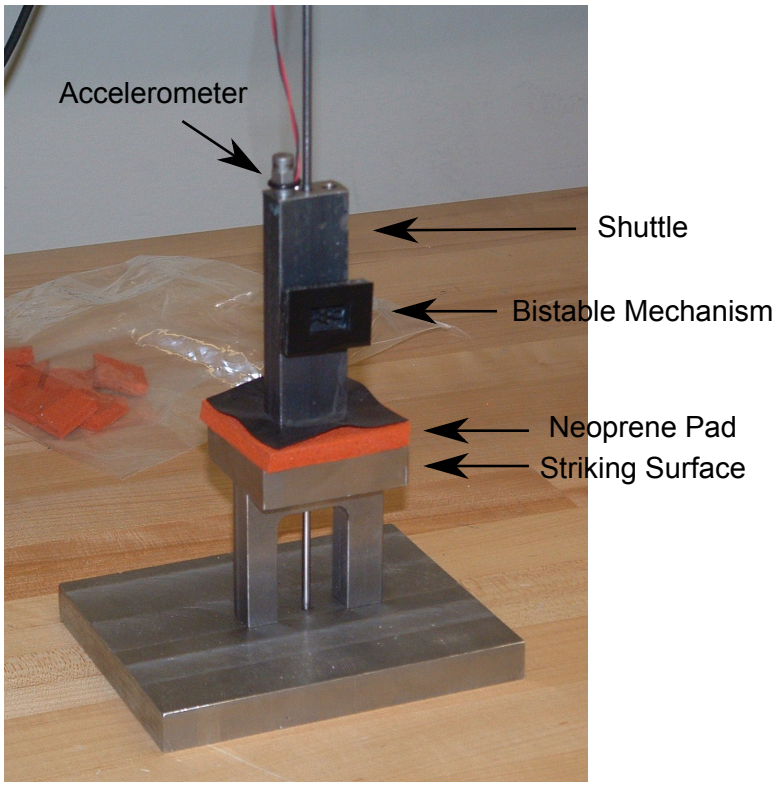

Figure 3.8: Drop Tester showing the shuttle, striking surface, accelerometer and bistable sensor.

Fourier transform was also performed in LabVIEW to verify the signal was clean and free of harmonics.

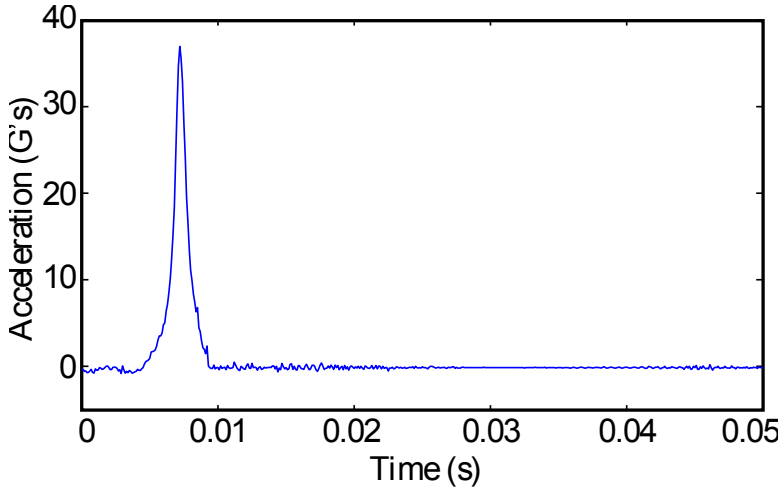

Figure 3.9: Typical drop acceleration pulse of the drop tester shown in Figure 3.8.

When tested in the centrifuge, the drop tester, and the shaker table, the RFID sensor behaved as expected and withstood all the acceleration loadings, which went as high as 500 G's. In all cases, the RFID reader reported back the correct state of the sensor after acceleration events by indicating either an inverted or non-inverted data stream. Several bistable shock sensors with varying frame weights were tested to find the required switching accelerations in each of the three testing environments. We were targeting switching accelerations in the 30-50 G range, since this is typical for shock sensors used in the shipping industry. Figure 3.10 shows the average centrifuge, shaker and drop test accelerations for five sensors of equal frame weights. The variations between the switches were likely due to the manufacturing of the switches. The laser cutting of the plastic caused melting and thus random variations in the switches, as described earlier.

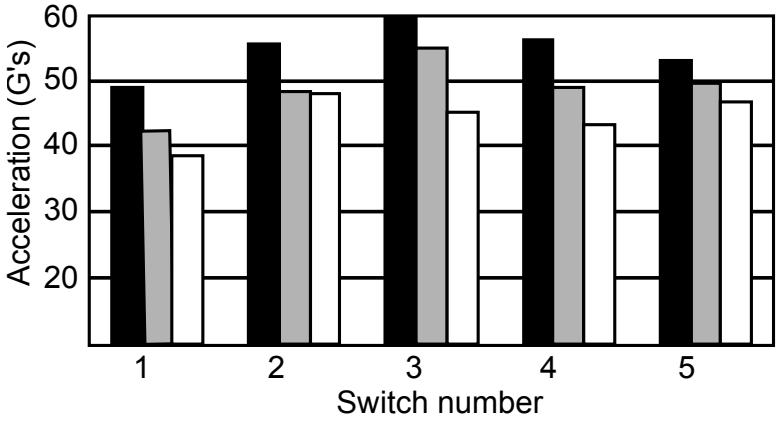

Figure 3.10: Average switching accelerations for five switches with the same mass. Drop test (Black), shaker test (Gray) and centrifuge (White)

We also used the shaker table to explore the frequency response of the sensors. To do this, we applied a sinusoidal acceleration at a specified frequency and increased the amplitude of the signal until the bistable mechanism switched. From Figure 3.11, we see that as the excitation frequency changes, the acceleration needed to flip the sensor changes slightly. This effect was further explored using a nonlinear dynamic model of the sensor. The sensor was modeled as a mass-spring-damper system, with a nonlinear spring force

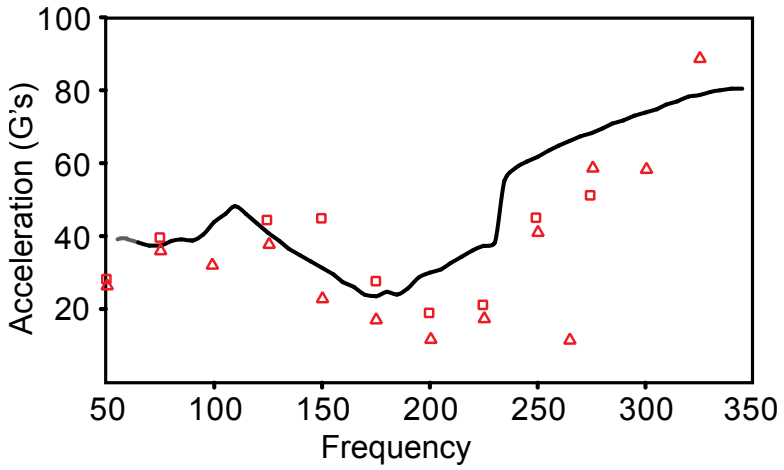

Figure 3.11: Frequency response of the sensor. The solid line indicates the predicted model response. The triangles and squares are two switches measured responses.

following the trend shown in Figure 3.2. The model equation was

$$m\ddot{x} + b\dot{x} + F_k(x) = b\dot{x}_{in} + F_k(x_{in}) \tag{3.3}$$

where m is the suspended mass of the sensor (4.4 g), x is the output displacement of the sensor, b is a damping coefficient (approximated as 1 Ns/m), $F_k(x)$ is the nonlinear bistable spring force, and x_{in} is the input motion of the shaker table. $F_k(x)$ was evaluated using a cubic spline interpolation of data from a finite element model of the mechanical device. To predict the frequency response using this model, x_{in} was set equal to $A\sin(\omega t)$, where A is the amplitude of motion and ω is the angular frequency. By varying the amplitude A for a particular frequency, we were able to determine the total acceleration A/ω^2 required to cause switching of the device. This process was repeated every 5 Hz over the range shown in Figure 3.11. As the figure shows, the model accurately predicts both the trend and magnitude of the frequency response over the range tested.

The shape of the frequency response is due to the non-linear behavior of the device. Figure 3.11 shows a resonant frequency for the device around 175 Hz. This explains the different G-forces between testing methods seen in Figure 3.10. The shaker test was performed at 100 Hz, while the centrifuge can be related to a low frequency input to the sensor. From the frequency response of Figure 3.11 we would expect the centrifuge thresh-

old G-force to be less than that for the shaker table. Similarly, the drop test corresponds to a high frequency input, and as such we would expect its switching force to be larger than the other two tests. These observations are validated by the data presented in Figure 3.10. Note that variation in the leg thickness due to the manufacturing process would also shift the resonant frequency as well as the switching accelerations for other frequencies.

3.6 Conclusion

A zero power, RFID-enabled shock sensor was developed and tested under three loading conditions. It was shown that in each of the three loading conditions the threshold switching accelerations were similar in magnitude. The threshold accelerations of the tested sensors varied between 28 and 50 Gs, and these values can be modified by changing the mass of our mechanical accelerometer. There was some variation in the switching thresholds for accelerometers of the same mass and design due to irregularities in the laser cutting manufacturing method. Less variation will likely be achieved with manufacturing methods with less variability, like injection molding. The frequency response of the sensors indicated that there is a resonance for the switches near 175 Hz, but that should be well above any vibration frequencies experienced in most shock monitoring applications. Sensor states were read using a commercially available RFID reader at a distance of 3 cm. This distance could likely be increased but would require an RFID chip operating at a high frequency with a sensor input.

Chapter 4

Variability and Materials

4.1 Variations

During testing of the plastic bistable mechanisms described in Chapter 3, significant variations were seen. Since these devices will be used as accelerometers, it is necessary to keep the variation in the devices to a minimum. Upon closer observation and study, it was found that most of the variation came from three sources. The first was stress relaxation in the plastic due to leaving the devices in a stressed state for an extended period of time. The second source of variation was temperature fluctuations of the devices. The third cause was that of manufacture variability. This chapter will look at and discuss reasons for these problems in the plastic devices. It will also address some other materials that might be used.

4.1.1 Stress Relaxation

The accelerometers created from Delrin were observed to have significant stress relaxation. Stress relaxation is defined as a gradual time-dependent deformation of a material due to a constant application of stress to a material [30]. In our application the compliant flexures of the bistable mechanism are put into the second stable position. In this position significant stress is maintained in the viscoelastic leg members, allowing stress relaxation to occur. However, this stress is needed to allow for the storage of energy. This energy storage is key in achieving the difference in activation forces desired as described in Section 3.3. Figure 4.1 shows a plastic bistable switch in its first (unstressed) and second (stressed) stable position. Testing for stress relaxation was done by drop-testing the bistable mechanisms in their second stable position to find the switching G-force. Next, the switches were

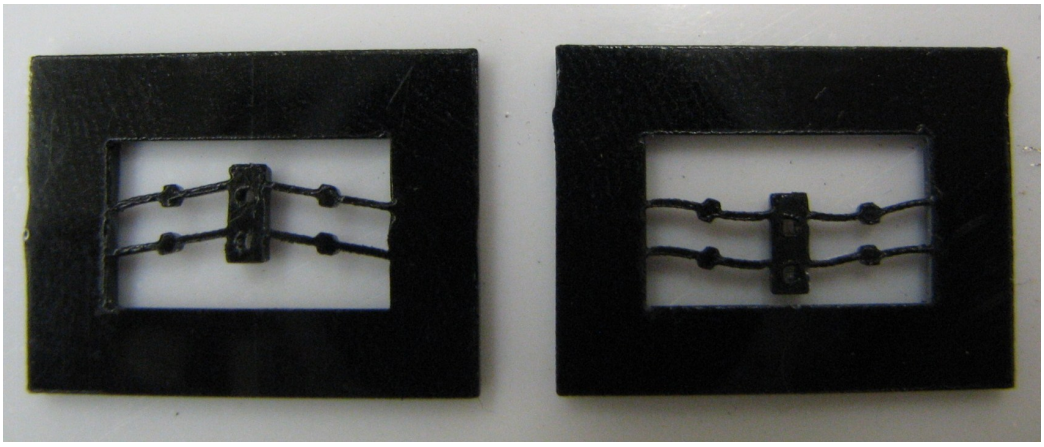

Figure 4.1: The first(left) and second(right) stable position of the Delrin bistable mechanisms showing highly flexed/stressed regions.

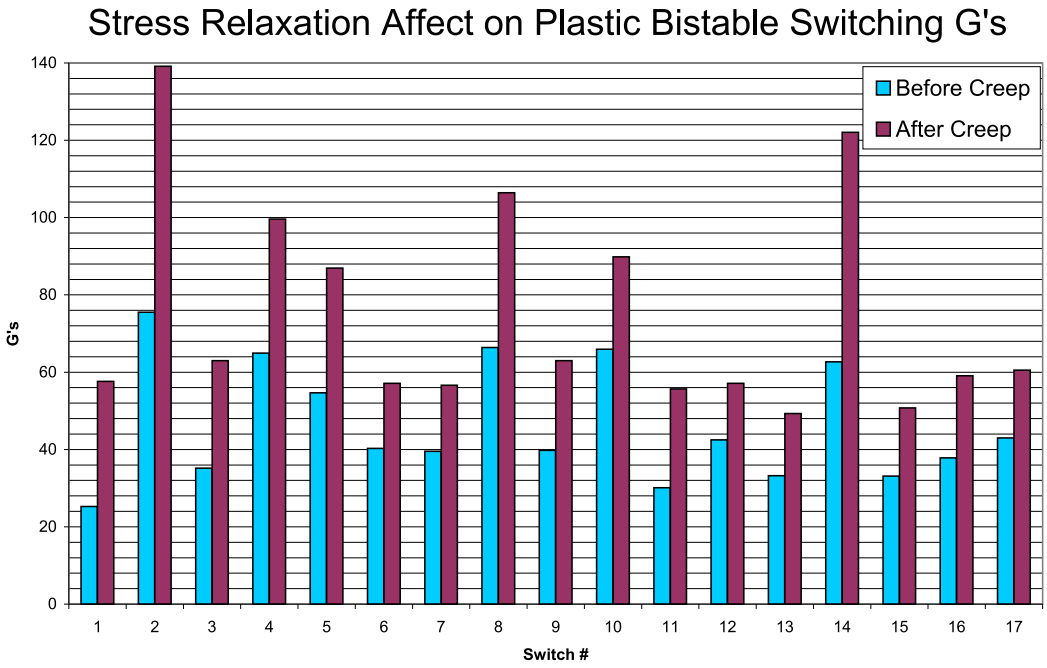

Figure 4.2: The drop test data showing the stress relaxation on the Delrin bistable mechanisms.

left in their second stable position for three days and then retested. As seen in Figure 4.2, the switching forces changed significantly. Taking the average of all the switches, it was found that the switching force increased by 53.5%.

With the application of a threshold accelerometer sensor in mind, this effect is detrimental. This indicates that even if the device were designed to switch at a desired threshold G-force, the device's switching threshold would change significantly while sitting in its

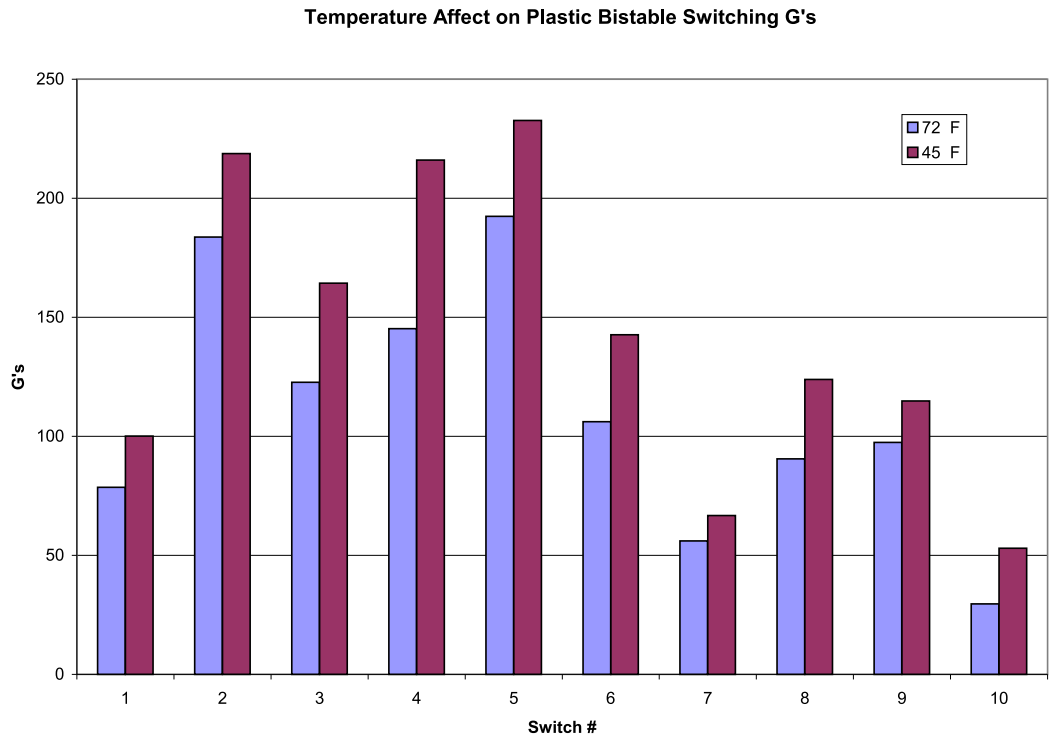

Figure 4.3: The drop test data showing the results of temperature on the Delrin bistable mechanisms.

second stable position, waiting for the threshold acceleration to be exceeded. This effectively eliminates the use of the device as an accurate threshold accelerometer. This must be overcome in order to have a commercially realizable device.

4.1.2 Temperature

Variation was observed in the device from differing temperatures. A drop test was performed to determine the switching G-force needed at a temperature of 72° F. The device's temperature was then dropped to 45° F by placing it into a refrigerator. The device was left there until the temperature reached an equilibrium. It was then immediately removed from the refrigerator and the test was quickly repeated. The variation in the switching force was observed to be 33.8% and is seen in Figure 4.3.

The change in temperature on the plastic has the effect of increasing or decreasing the pliability of the material. As such, the forces needed to switch the device to the other stable position can increase or decrease. This effect could also be tied to the stress relaxation described earlier. The speed at which the material will relax due to stress is dependent

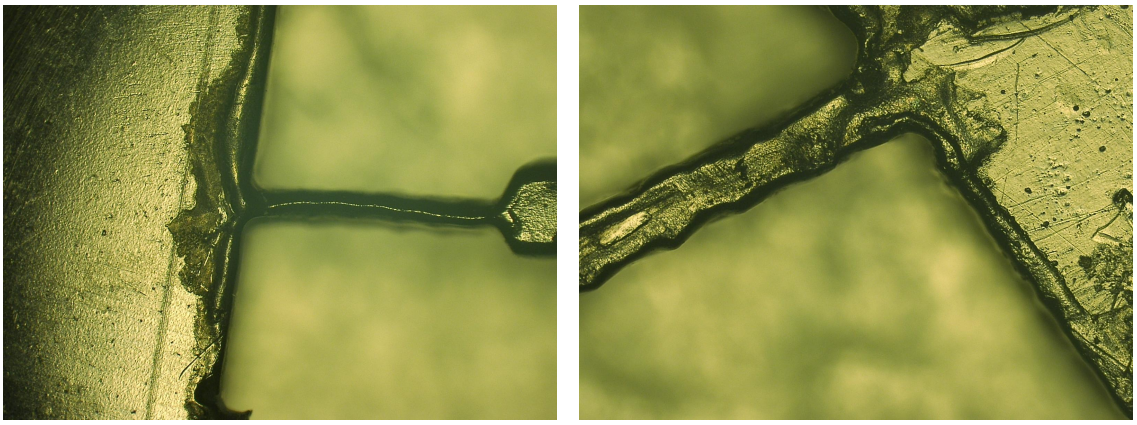

(a) The top view of a laser cut compliant flexure. (b) The bottom view of a laser cut compliant flexure.

Figure 4.4: Variability and beading of the compliant flexures due to laser cutting.

on the temperature of the device as well as the stresses experienced [31]. The higher the stress and the temperature, the faster stress relaxation will occur. Since this device will need to work in varying temperatures, this attribute is not desirable and needs to be reduced or eliminated.

4.1.3 Manufacturing

Manufacturing of the devices themselves induced significant variation as briefly mentioned in Section 3.4. This variation was measured to be 10.4% for devices of the same mass and leg widths. The issue can be better seen in magnified pictures as shown in Figure 4.4. The top of the device's compliant legs have melted from the laser cutting process as seen in Figure 4.4(a) and the bottom has remained fairly flat except for slight beading along the edge, as seen in Figure 4.4(b). This variation in the cross-section changes the force and displacement characteristics expected in the compliant flexures.

Not only does the cross-sectional form change from the top to the bottom, but it also changes along the length of the compliant flexure as seen in Figure 4.5. This variation will change how the compliant member bends and will affect the switching G-force of the device. This also causes the compliant legs in the mechanism to not match each other in the force exerted on the opposite compliant flexure, leading to asymmetry during motion.

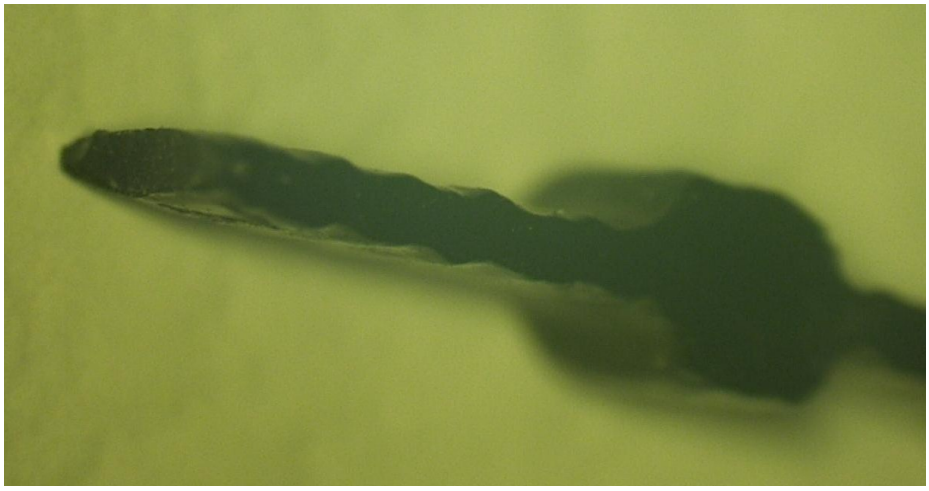

Figure 4.5: Close up picture of a compliant flexure with width variations along its compliant legs.

4.2 Materials

Several different types of plastics were formed into bistable devices to determine if they improved the Delrin plastic design. These types of plastics included acrylics, ABS, polypropylene and polycarbonate [29]. Each of these proved to be more difficult to manufacture. The acrylics were very brittle and did not allow for the compliant flexures to deflect as far as needed before breaking. The ABS had even more melting/beading variation from the laser cutting than the Delrin and had higher stress relaxation issues. Beyond these issues, J. Bicerano notes in his book "Predictions of Polymer Properties" [32]

> Since the durability of a plastic article under use conditions depends strongly on the viscoelastic processes, there are major challenges facing researchers who want to develop the ability to predict durability under use conditions where a plastic article is often exposed to considerably more complex temperature and deformation histories than encountered in typical laboratory experiments.

Since the goal is to have an accurate sensor, another material will need to be chosen to create a threshold accelerometer.

Ceramics were looked at as a possible replacement. However, these materials are very brittle. This would require the compliant flexures to be thin and longer, making the device large and minimizing the environments it could be placed in. It was determined

that metals would be a better material to use in that they have less stress relaxation and temperature variations when compared to plastics. They are flexible, if designed properly, and have high strengths. The drawback with using metals is the difficulty of fabricating thin compliant flexures accurately and inexpensively.

Chapter 5

Design and Testing of a Thin-Flexure Bistable Mechanism Suitable for Stamping from Metal Sheets

5.1 Introduction

[1] Compliant mechanisms are mechanisms where the structural members are allowed to flex or bend to allow for motion of the mechanism [15]. As these members flex due to some external force, elastic energy is stored in the members. Compliant mechanisms allow for mechanisms to be created from a single piece of material with no joints or assembly. For a variety of reasons, compliant mechanisms are often made from plastics. Plastic offers low manufacturing costs and a relatively high ratio of strength to Young's modulus [33]. However, when accuracy and repeatability are important in an application involving compliant mechanisms, special considerations must be taken into account. For many applications, metal is ideal over other materials, such as plastic, as it has better predictability of its material properties, and there is less variation in the material, allowing for less variation in the performance of the manufactured parts. Another advantage of metal over a plastic material is the stress relaxation characteristics. Metal can remain in a stressed state for long periods of time and not lose its stored elastic energy. Plastics will lose this energy due to stress relaxation in the plastic material. Disadvantages of using metals include the high cost compared to plastics and the inability to manufacture thin flexures easily. Compliant mechanisms made from metal have been previously fabricated using machining [34], stamping [34,35], bending of sheets [36,37], wire EDM [38–40], bending of wire [41] and laser cutting [35]. However, none of these previous methods has allowed fully compliant mechanisms with extremely thin flexures.

[1] This Chapter is a paper that has been prepared for submission to the ASME Journal of Mechanisms and Robotics and was co-authored by Stephen M. Schultz, Aaron R. Hawkins and Brian D. Jensen

This paper presents a new method for designing compliant mechanisms that allows thin flexures to be easily and inexpensively made in metal from a single stamping or fine blanking process. The method leads to a unique design for a fully compliant bistable mechanism used as a threshold acceleration sensor. A model of the bistable mechanism is presented. Data showing low variation and resistance to stress relaxation and temperature effects for the acceleration sensor is also shown.

5.2 Concept

Compliant mechanism design often requires flexures with small widths compared to their lengths. Therefore, if small overall size is desired, width must be as small as possible. Unfortunately, low-cost metal forming methods such as stamping are limited in the minimum achievable dimensions. Typical minimum widths for this process are 0.06 inches (1.524 mm) with a typical tolerance of $\pm$0.001 inches (0.0254 mm) although minimum widths as small as 0.006 inches (0.1524 mm) are achievable with higher cost [42]. To make a compliant member at the minimum size using these process parameters, the width could vary $\pm$16.7% with the indicated tolerance, creating variation in the deflection or force of the flexure.

To overcome this difficulty, we propose a new method to fabricate ultra-thin flexures in stamped metal parts. If the sheet were made very thin, then the compliant member could be bent out of the plane of sheet by 90°. The width would then have the properties of the thickness of the thin sheet of material as seen in Figure 5.1. A typical 0.004 inch (0.1016 mm) steel sheet can be readily purchased with a thickness tolerance of 0.0005 inches (0.0127 mm). This would result in a width variation of only $\pm$12.5% without having to push the envelope on the fabrication processes abilities. This would reduce the cost, variation over time due to wear of the fine blanking tooling, and the defect count.

During design, two considerations for stress must be made. First, the material must yield but not fracture at the rotation points to keep the flexible member 90° out of plane. Secondly, the compliant member cannot yield throughout its range of motion. These considerations require more work in the initial design, but give greater benefits in reducing the size of the compliant device.

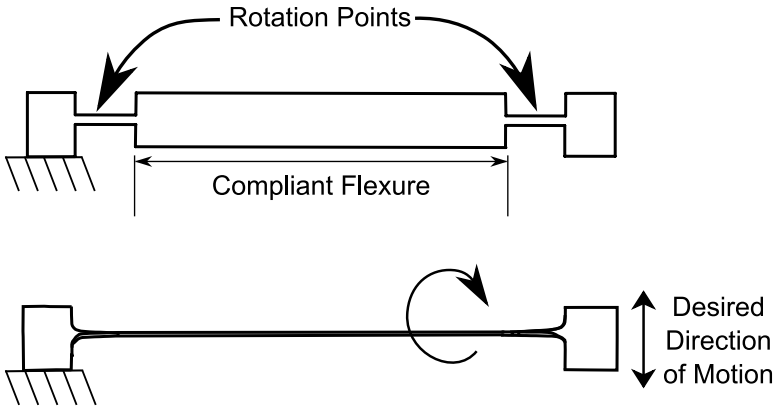

Figure 5.1: Diagram showing a thin sheet bent out of plane 90° to create a compliant flexure.

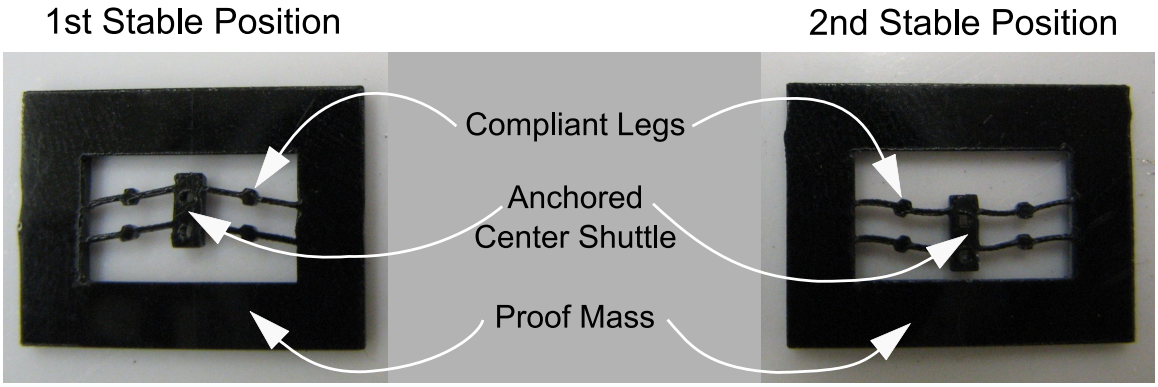

Figure 5.2: Bistable design showing the 1st and 2nd stable positions, proof mass, compliant legs and anchored center shuttle.

5.3 Design

Earlier work has been done in designing a fully-compliant bistable mechanism as a threshold accelerometer as discussed in Chapter 3. This device uses four compliant flexible members and is designed to have two stable positions as seen in Figure 5.2. This device is based on the Fully Compliant Bistable Mechanism (FCBM) presented by Parkinson et al. [28] When an acceleration is experienced, the proof mass, or outer frame, will cause a force to be placed on the compliant legs allowing the device to switch between the first or second stable position. This mechanism was originally made from Delrin and was fabricated by laser cutting. During testing of the plastic device, it was found that the force needed to deflect the device was changing over time. This occurred when the device was left in its second stable position, leaving the compliant members in stressed positions which

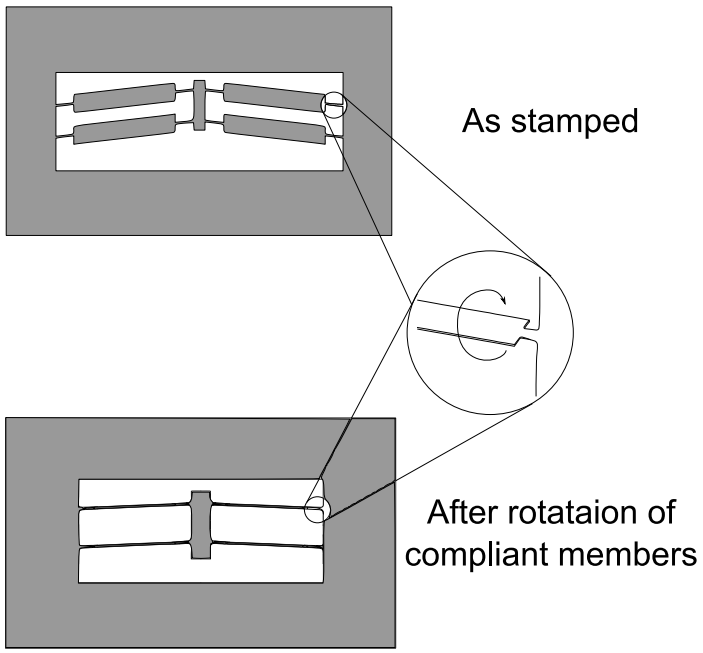

Figure 5.3: The bistable design showing the compliant members bent about the center of axis.

caused the plastic material to relax its stresses, losing some of its stored energy. Temperature changes also caused variation in the switching force. Beading of the thin flexural compliant legs from the laser cutting fabrication process also induced significant variation, changing the force versus displacement characteristics that were expected. This type of device is an ideal candidate for the fabrication method presented in this paper. With this method one should get low stress relaxation and little variation in the forces with changes in temperatures. The new design has straight flexible legs with no rigid segment, unlike the FCBM design. Therefore a new model is required to describe this mechanisms behavior.

The proposed concept rotated the compliant legs about the center of the compliant flexures as seen in Figure 5.3, allowing the metal to yield at the thinned rotation points of the design.

5.3.1 Straight-Leg Bistable Mechanisms

The new bistable mechanism design, called the Straight-Leg Bistable Mechanims (SLBM), is pictured in Figure 5.4. In this bistable mechanism, each leg (of length L) is placed at an angle γ with respect to the horizontal. Because of symmetry, only one such leg

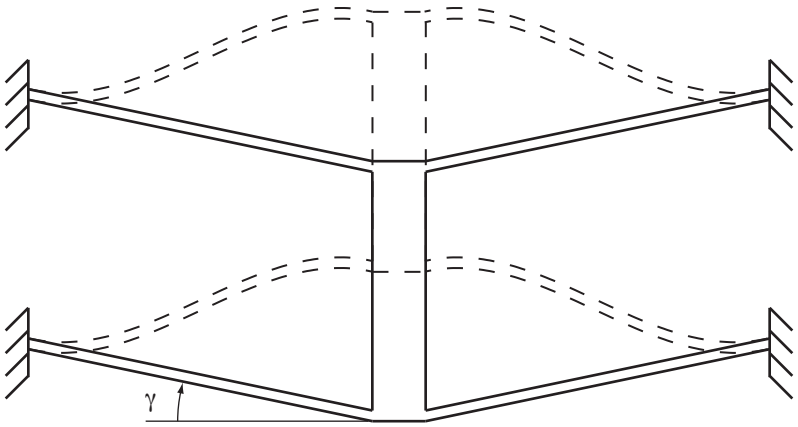

Figure 5.4: An illustration of a straight-leg bistable mechanism (SLBM), with both stable positions shown.

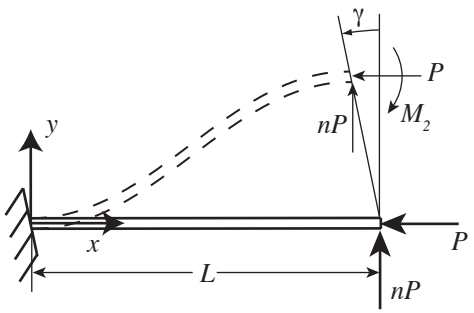

Figure 5.5: A diagram showing one flexible beam being deflected by end forces and moments. To model the motion of a SLB, the beam's end must traverse a line at an angle γ with respect to the vertical.

needs to be modeled. By rotating the axes so that the x-axis lies along the beam's length, the motion of the SLBM can be modeled as a motion of the beam's end along a line tilted by an angle γ with respect to the y-axis. Figure 5.5 illustrates such a motion. The end angle of each end of the beam is constrained to be zero with respect to the x-axis. Under these constraints, the problem becomes one of finding the end forces, P and nP, and the end moment, M_2, that cause motion along the given line.

This problem may be solved using the elliptic integral methods of Shoup and McLarnan [43]. The solution requires the introduction of two new variables, k and ϕ, which represent the modulus and amplitude of the elliptic integral functions used in solution. Using the boundary conditions described above, the equations required for solution can be written

in non-dimensional form as

$$\sin\phi_1 = \sqrt{\frac{\eta - 1}{2k^2\eta}} \tag{5.1}$$

$$\sin\phi_2 = \sin\phi_1 \tag{5.2}$$

$$\alpha = \frac{1}{\sqrt{\eta}}\left[F(k,\phi_2) - F(k,\phi_1)\right] \tag{5.3}$$

$$\frac{a}{L} = \frac{1}{\alpha\eta^{\frac{3}{2}}}\left[2E(k,\phi_2) - 2E(k,\phi_1) - F(k,\phi_2) + F(k,\phi_1) - 2nk(\cos\phi_2 - \cos\phi_1)\right] \tag{5.4}$$

$$\frac{b}{L} = \frac{1}{\alpha\eta^{\frac{3}{2}}}\left\{n[2E(k,\phi_1) - 2E(k,\phi_2) - F(k,\phi_1) + F(k,\phi_2)] + 2k(\cos\phi_1 - \cos\phi_2)\right\} \tag{5.5}$$

where

$$\eta = \sqrt{1+n^2} \tag{5.6}$$

$$\alpha = L\sqrt{\frac{P}{EI}} \tag{5.7}$$

and $F(k,\phi)$ is the elliptic integral of the first kind, and $E(k,\phi)$ is the elliptic integral of the second kind. In addition, a and b are the x- and y-direction coordinates of the end of the beam, E is the Young's modulus of the material, and I is the second moment of area of the beam's cross-section. For motion along the line with angle γ to the vertical, a and b are known, and the problem becomes one of finding the appropriate n, k, and α to satisfy the equations. Because the equations are nonlinear, this requires a numerical solution.

Some consideration must be given to the relative values of ϕ_1 and ϕ_2. Obviously, one solution to Equation (5.2) is $\phi_2 = \phi_1$. However, this solution may be considered a null solution because it results in no deflection or force. In fact, though, there are infinitely many solutions to the equation. The first two are

$$\phi_2 = \pi - \phi_1 \tag{5.8}$$

$$\phi_2 = 2\pi + \phi_1 \tag{5.9}$$

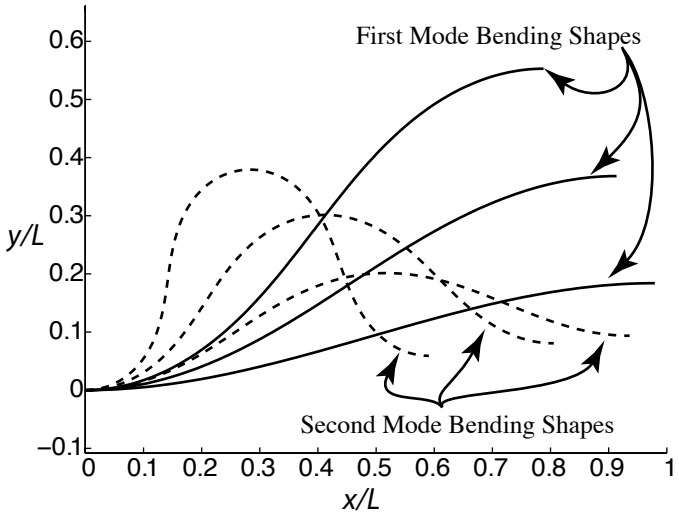

Figure 5.6: A plot showing the basic shape of the first and second modes of bending.

These two solutions correspond to the first and second modes of bending, illustrated in Figure 5.6. Note that the first mode has an inflection point at the center of the beam, while the second mode has two inflection points distributed about the center of the length. Higher-order mode shapes exist, of course, but they will not be seen in real static deflections.

The equations above are sufficient to describe the bending behavior of the beam, assuming inextensible beams. However, large axial forces in the beam could induce axial strains, which must also be accounted for. The axial strain at any point along the beam is

$$\varepsilon_{axial} = \frac{F_{axial}}{EA} = \frac{P\cos\theta - nP\sin\theta}{EA} \tag{5.10}$$

where F_{axial} is the axial force, θ is the angle of the beam with respect to the x-axis, and A is the cross-sectional area. Integrating the x- and y-components of strain along the length of the beam gives the additional non-dimensionalized deflection due to axial strains:

$$\frac{\Delta a}{L} = \frac{\alpha^2}{S^2}\int_0^1 (\cos^2\theta - n\sin\theta\cos\theta)\mathrm{d}s_l \tag{5.11}$$

$$\frac{\Delta b}{L} = \frac{\alpha^2}{S^2}\int_0^1 (\cos\theta\sin\theta - n\sin^2\theta)\mathrm{d}s_l, \tag{5.12}$$

where s_l is the non-dimensionalized coordinate along the beam length and S is the slenderness ratio, defined as

$$S = L\sqrt{\frac{A}{I}} = \frac{L}{k} \tag{5.13}$$

with k the radius of gyration for the beam cross section. Assuming that the overall deflection is not significantly affected by the axial strain, both θ and s_l can be given as functions of k, ϕ, and α as

$$\theta = 2[\sin^{-1}(k\sin\phi) - \sin^{-1}(k\sin\phi_1)] \tag{5.14}$$

$$s_l = \frac{1}{\alpha\sqrt{\eta}}[F(k,\phi) - F(k,\phi_1)] \tag{5.15}$$

where ϕ varies between ϕ_1 and ϕ_2 along the beam's length. Equations (5.11) and (5.12) may most conveniently be evaluated numerically, using the relationships in Equations (5.14) and (5.15). Considering both beam bending and axial strains, the coordinates for the beams end are then $(a-\Delta a, b-\Delta b)$.

Further, the stress along the beam, which is a combination of axial stress and bending stress, can be found from

$$\frac{\sigma}{E} = \frac{\alpha^2}{S^2}(\cos\theta - n\sin\theta) + \beta\frac{c}{L} \tag{5.16}$$

where c is the largest perpendicular distance from the neutral axis of the beam to its surface, and β is the nondimensionalized moment, given by

$$\beta = \frac{ML}{EI} \tag{5.17}$$

and M is the bending moment in the beam. β is given by (see [43])

$$\beta = 2k\alpha\sqrt{\eta}\cos\phi \tag{5.18}$$

For modeling motion of a SLBM, the beam's end must follow the line with an angle of γ with respect to the y-axis (see Figure 5.5). Hence, a and b are related by

$$a = L - b\tan\gamma \tag{5.19}$$

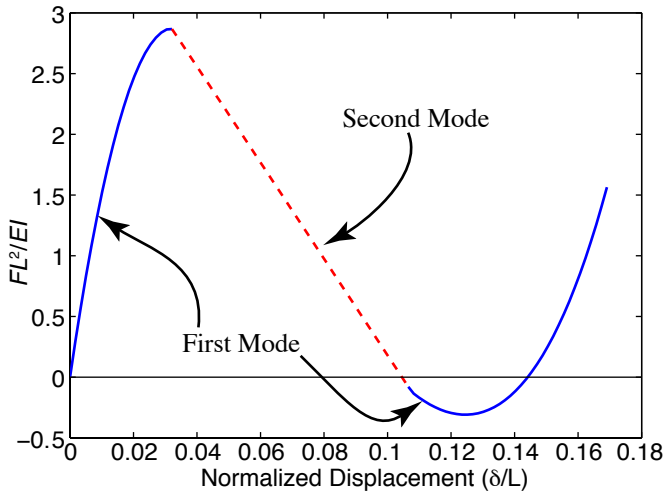

Figure 5.7: A sample model force-displacement curve for a single beam with $S = 123.7$ in a SLBM with $\gamma = 6°$

and the problem becomes one of finding the appropriate k, n, and α to meet the constraint in Equation (5.19). Both bending modes must be considered in the solution. Then, the force F acting along the line, which corresponds to the force that creates motion in the bistable mechanism, is

$$F = P(n\cos\gamma + \sin\gamma) \tag{5.20}$$

The entire solution was implemented in MATLAB. A sample force-displacement profile for a single leg in a SLBM with $\gamma = 6°$and $S = 123.7$ is shown in Figure 5.7. The figure notes which part of the solution corresponds to both first and second mode bending. The part of the solution corresponding to the first mode qualitatively behaves like the force-displacement plot of a Fully Compliant Bistable Mechanism (the name given to the bistable mechanism design incorporating the rigid segments, see [28]). However, the second mode solution behaves very differently, giving a straight line to the force-displacement curve. This model will be used in the design of our device.

5.3.2 Device Design

In designing the device, the material's elastic limit, yield strength and fracture strength had to be taken into consideration. The design required the yielding of the material in the rotation segments to keep its shape in the proper position once manufactured.

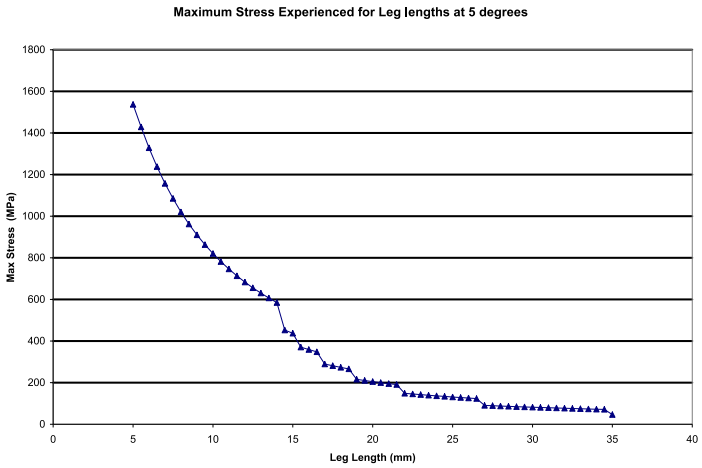

Figure 5.8: Stress calculated for leg lengths at a 5° angle using the elliptic integral model.

However, the compliant legs of the device must be designed to not yield in its range of motion, so the device would not have variation in the switching forces required. In this design a 1095 spring steel that was 0.004 inches (0.1016 mm) thick was used. The yield stress for this particular material is 760 MPa and fracture occurs at 1360 MPa [44]. Using the straight-leg bistable mechanism model, two designs were chosen for fabrication with leg lengths of 20.5 mm and 25 mm and an angle of 5°. This allowed the device to be bistable while keeping the stresses well below the yielding stress for the compliant flexures as seen in Figure 5.8. These dimensions also allowed the device to have a robust, bistable force-displacement profile. For the yielding flexures at the rotation points, finite element analysis 5was used to determine the length and width needed to allow for yielding, but not cause fracture. In this case, the flexures were 2.5 mm (0.0984 inches) long and 0.4 mm (.016 inches) wide, giving a maximum stress of 1282 MPa as seen in Figure 5.9.

5.3.3 Prototypes

The cost of creating a die for fine blanking prevented us from using this method for fabrication, so prototypes were made using a wire EDM process. The prototype before and after yielding the flexures is shown in Figures 5.10 and 5.11. As can be seen in Figure 5.11, a constraining band has been placed on the shuttle to keep the legs in-plane when actuated. Out-of-plane motion has been determined to cause wide fluctuations in the switching forces [45].

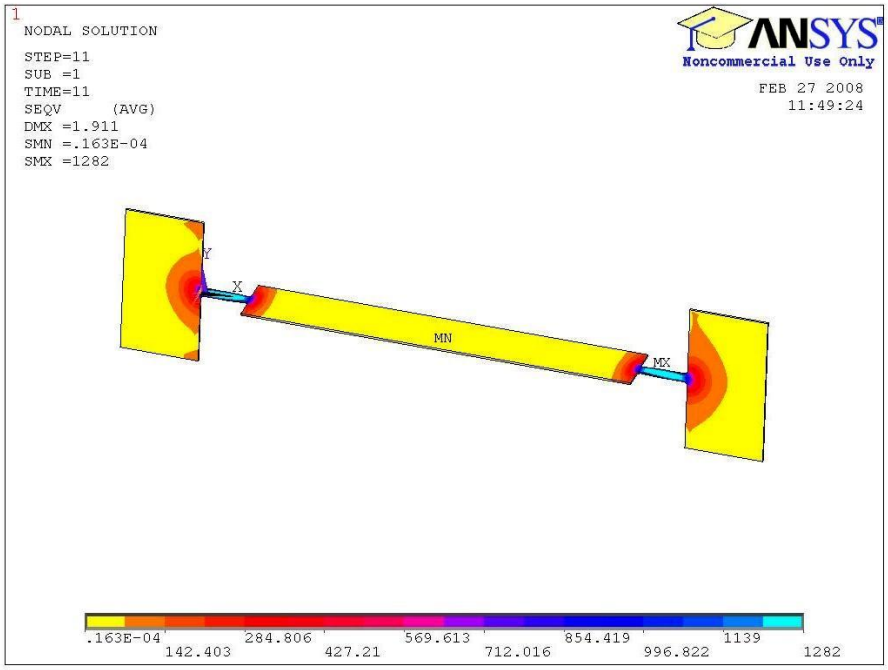

Figure 5.9: Bistable design showing the stresses in MPa from the ANSYS model for yielding at the rotation points.

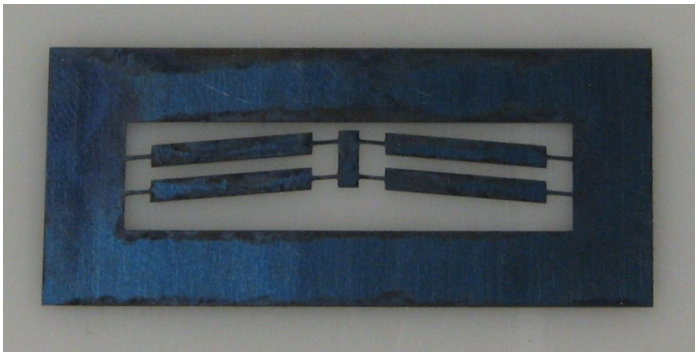

Figure 5.10: Bistable prototype shown before yielding the flexures by twisting about the center of axis.

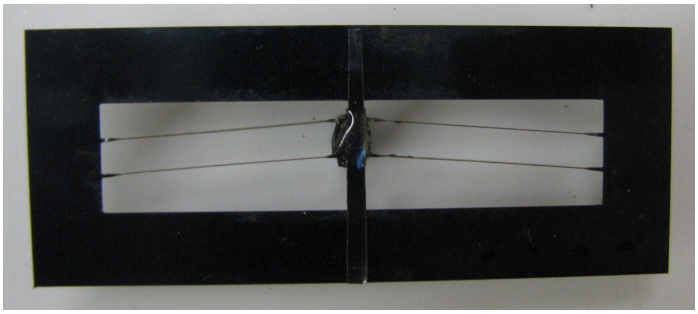

Figure 5.11: Bistable prototype shown after yielding the flexures by twisting about the center of axis.

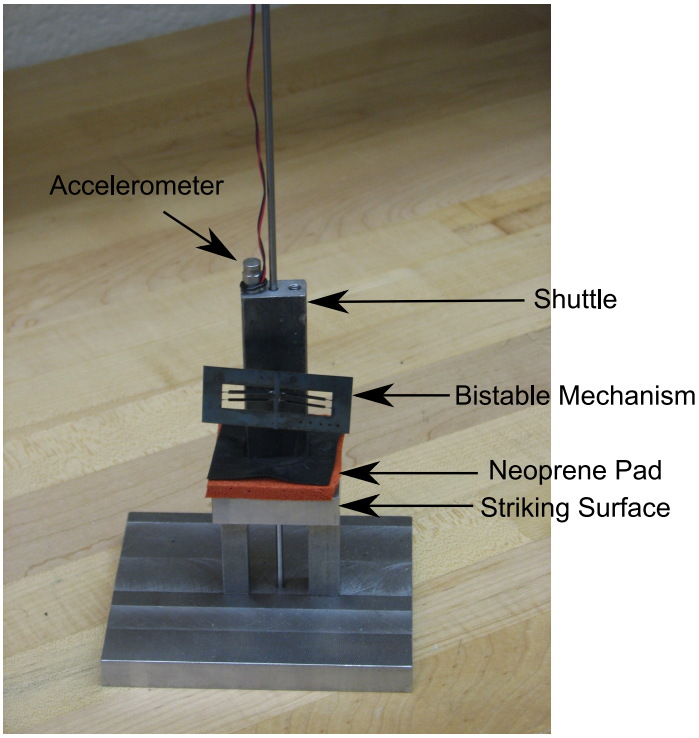

Figure 5.12: Drop test setup showing the bistable device, the shuttle, accelerometer and the impact platform.

5.4 Testing

The acceleration threshold for switching of each design was tested using a drop test. This test was performed by anchoring the center shuttle of the bistable device onto a steel runner, which was then dropped onto a steel platform with a layer of neoprene as a cushion, as seen in Figure 5.12. An accelerometer was mounted onto the steel runner, and G-forces were measured to determine the switching force. The devices were first tested to determine the G-force needed to switch the mechanism from its second stable position to the first stable position. The devices were then left in the stressed second stable position for three days time and then retested to determine if any stress relaxation of the material had occurred. With the plastic Delrin bistable switches, the average change in switching G-force after stress relaxation was measured to increase by 53.5%. With the metal design, the average change in switching G-force increased by 2.05%, which is within the variation of the measured switching forces. A temperature variation test was also performed. This test was conducted by bringing the temperature down from room temperature at 72° F to 45° F

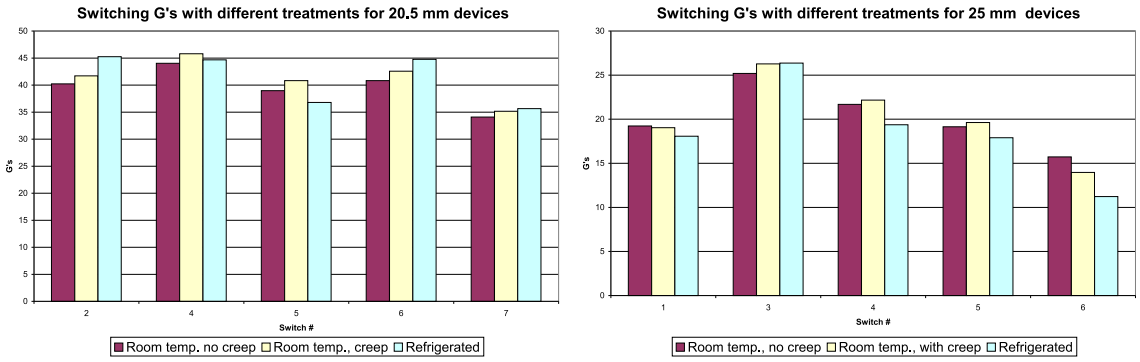

(a) 20.5 mm Switching G's. (b) 25 mm Switching G's.

Figure 5.13: The measured average switching G's for the 20.5 and 25 mm bistable devices.

in a refrigerator and testing the bistable switching force. The average change in switching G-force was measured to be 2.5%, which is within the variation of the measured switching forces. The plastic bistable mechanism's measured change for the same test was much more significant at 33.8%. The data for switching of the metal bistables is summarized in Figure 5.13.

The model predicted that the switching force from the second stable position to the first stable position for the bistable device with leg length of 20.5 mm would be 45.3 G's while the bistable device with a leg length of 25 mm was predicted by the model to switch at 29.6 G's. The measured results found the actual switching forces to be lower at 39.3 G's for the 20.5 mm leg length design and 21.6 G's for the 25 mm leg length design. These values can vary due to different excitation frequencies. In order to explore frequency response, we tested the devices using a shaker table. We applied a sinusoidal acceleration at a specified frequency and increased the amplitude of the signal until the bistable mechanism switched. The frequency response results of the switch are shown in Figure 5.14.

In order to better understand the behavior of the device, its force was measured as a function of displacement. This was done by mounting the device to a force transducer, specifically an Interface Force S-Beam type, strain gage based load cell. This was then attached to a screw type tensile/compression tester with a counter weight to keep the forces measured in the positive region. The force was measured as the device was moved from the second stable position to the first stable position. The data is shown in Figure 5.15.

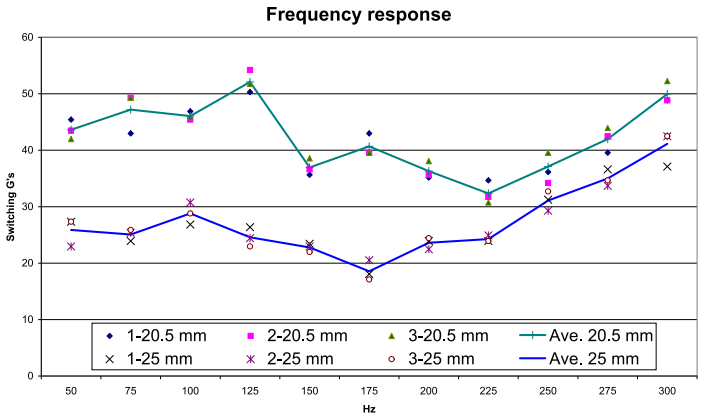

Figure 5.14: The measured frequency responses for the 20.5 and 25 mm bistable devices.

Twisting of the legs during fabrication caused their initial angle to decrease slightly from the designed 5°. After twisting the legs into the proper position, the leg angles were measured and found to be 4.33°. Figure 5.15 also shows the predicted curve for a compliant beam of 25 mm length at an angle of 4.33°. The model predicts the first stable, second stable and unstable equilibrium positions fairly accurately. However, the force magnitudes do not match. As mentioned earlier, we believe this is due to out-of-plane motion in the device. The measured force required to switch from the second to the first stable position (135 mN) corresponds to a switching acceleration of 14.7 G's, a 32 % drop from the average of the drop test data. We believe that the counter weight attached to the switch during force-displacement testing caused asymmetric loading on the switch, reducing the measured switching force. See [45] for modeling showing a similar effect.

5.5 Conclusion

This paper has presented a new method for fabricating compliant mechanisms that allow thin flexures to be easily and inexpensively made in metal from a single stamping or fine blanking process. A model of the bistable mechanism was presented that uses the elliptic integral solutions for beams in bending. The fabrication method and model were used to design a fully compliant bistable mechanism made from metal. This design was used as a threshold accelerometer sensor that was tested and compared to a plastic fully compliant bistable mechanism. Data was presented showing low variation and resistance

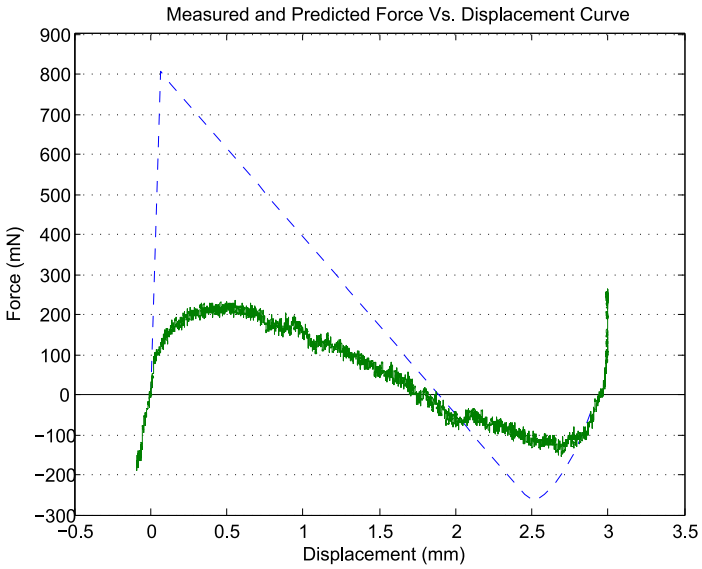

Figure 5.15: The predicted and measured force versus displacement curve for the 25 mm bistable devices at 4.33°.

to stress relaxation and temperature effects compared to the plastic acceleration sensors. It was also shown that the elliptic integral model predicts the motion of the device fairly accurately and can be used in the design of straight-leg compliant flexures.

Chapter 6

Conclusions and Recommendations

6.1 Conclusions

Chapter 3 has shown a threshold accelerometer has been successfully fabricated and integrated with a passive RFID tag. This in turn has been successfully read with an RFID reader and shown to act as a wireless passive sensor indicating whether or not a threshold acceleration has been exceeded. Multiple methods for testing the switching forces of these threshold accelerometers have been developed and a frequency response for the switching forces of these devices has been explored.

Chapter 4 has explored some different materials. It was shown that plastic is not a suitable material to use in threshold accelerometers due to variability in fabrication, temperature and prolonged stresses inducing stress relaxation in the material.

Chapter 5 introduced a straight-leg bistable design model. This design model was used to design metal bistable devices to reduce the variations seen in the plastic threshold accelerometers. With this metal design a new fabrication process was introduced to attain thin metal compliant flexures with little variation in the thickness of the compliant flexures. This method also allowed for a more economical method of producing these compliant flexures.

Chapter 5 also compared the metal bistable mechanism designs to the plastic bistable design and showed significant improvement over the plastic bistable designs. These improvements included minimizing the effects of stress relaxation, minimizing variation in switching forces and minimizing variation between fabricated devices. The cost, however, with the metal bistable design would be more than the plastic bistable design.

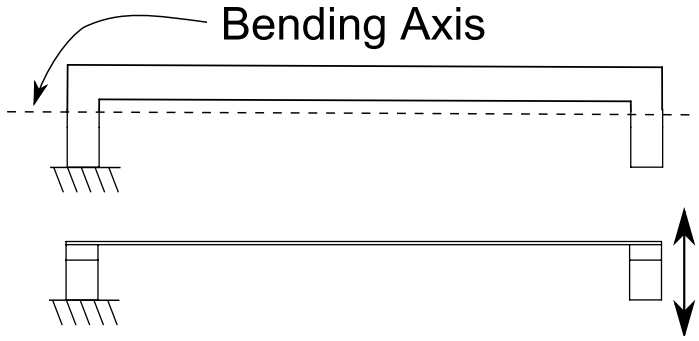

Figure 6.1: Proposed method for fabricating accurate compliant flexures from metal.

6.2 Recommendations for Future Research

This research has made many strides in the development of threshold accelerometers, yet there is much that still can be done in improving the devices. The first of these is bi-directional sensing. Currently these devices are designed to only sense an acceleration in one direction. There has been some work done in developing tristable devices that could be used to sense accelerations in both a positive and negative direction. These could be explored to determine how to integrate these devices with a passive RFID tag with proper acceleration ranges.

Related to bi-directional sensing is the need to develop an array of threshold accelerometers that would switch at multiple threshold accelerations. This would allow one to determine ranges of acceleration experienced. Putting these arrays into the three directional planes would allow sensing of off-axis accelerations, giving a much greater sensing capability

Another method for fabricating the metal compliant flexures has been explored, but needs to be looked at further. This method bends the flexures out of the plane of sheet metal 90 degrees instead of twisting the metal at rotation points as seen in Figure 6.1 This method is expected to increase the out-of-plane stiffness of compliant flexures compared to the twisting method presented in Chapter 5. Since the metal devices in Chapter 5 were constrained by gluing a thin metal strip onto the shuttle to keep the shuttle in-plane, this other method should decrease variation in the constraints and minimize the device-to-device variation seen in the devices of Chapter 5.

Finally, further work is needed to miniaturize the threshold accelerometers. The smaller these devices can be made and integrated into passive wireless communication, the more applications they can be used in. For example, if the devices could be fit into a typical integrated circuit package the device could be placed discretely in many different locations and used in many more applications.

References

[1] Tuttle, J., 8-11 Jun 1997. "Traditional and emerging technologies and applications in the radio frequency identification (RFID) industry." *Radio Frequency Integrated Circuits (RFIC) Symposium, 1997., IEEE*, pp. 5–8.

[2] Weinstein, R., May-June 2005. "RFID: a technical overview and its application to the enterprise." *IT Professional,* **7**(3), pp. 27–33.

[3] Akinci, B., Patton, M., and Ergen, E., 2002. "Utilizing radio frequency identification on precast concrete components suppliers perspective." *International Symposium on Automation and Robotics in Construction, 19th (ISARC). Proceedings. National Institute of Standards and Technology, Gaithersburg, Maryland.*, September 23-25, pp. 381–386.

[4] De Vita, G., and Iannaccone, G., Sept. 2005. "Design criteria for the RF section of UHF and microwave passive RFID transponders." *Microwave Theory and Techniques, IEEE Transactions on,* **53**(9), pp. 2978–2990.

[5] Radiom, S., Vandenbosch, G., and Gielen, G., 2008. "Impact of antenna type and scaling on scavenged voltage in passive RFID tags." *Antenna Technology: Small and Smart Antennas Metamaterials and Applications, 2007. IWAT '07. International Workshop on*, 4-6 March, pp. 442 – 445.

[6] Want, R., April 2004. "Enabling ubiquitous sensing with RFID." *Computer,* **37**(4), pp. 84–86.

[7] Glidden, R., Bockorick, C., Cooper, S., Diorio, C., Dressler, D., Gutnik, V., Hagen, C., Hara, D., Hass, T., Humes, T., Hyde, J., Oliver, R., Onen, O., Pesavento, A., Sundstrom, K., and Thomas, M., Aug. 2004. "Design of ultra-low-cost UHF RFID tags for supply chain applications." *Communications Magazine, IEEE,* **42**(8), pp. 140–151.

[8] Nambi, S., Nyalamadugu, S., Wentworth, S. M., and Chin, B. A., 2003. "Radio frequency identification sensors." In *Proc. 7th World Multiconf. Systemics, Cybernetics, & Informatics (SCI2003)*, pp. 386–390.

[9] Milos, F. S., Watters, D. G., Pallix, J. B., Bahr, A. J., and Huestis, D. L., 2001. "Wireless subsurface microsensors for health monitoring of thermal protection systems on hypersonic vehicles." *SPIE 6th Annual International Symposium on Health Monitoring and Diagnostics; United States*, 4-8 March.

[10] Opasjumruskit, K., Thanthipwan, T., Sathusen, O., Sirinamarattana, P., Gadmanee, P., Pootarapan, E., Wongkomet, N., Thanachayanont, A., and Thamsirianunt, M., Jan.-March 2006. "Self-powered wireless temperature sensors exploit RFID technology." *Pervasive Computing, IEEE,* **5**(1), pp. 54–61.

[11] Smith, J., Jiang, B., Roy, S., Philipose, M., Sundara-Rajan, K., and Mamishev, A., 2005. "ID modulation: Embedding sensor data in an RFID timeseries." In *Information Hiding: 7th Intl. Workshop*, Vol. 3727, pp. 234–246.

[12] Siden, J., Koptioug, A., and Gulliksson, M., 6-11 June 2004. "The "smart" diaper moisture detection system." *Microwave Symposium Digest, 2004 IEEE MTT-S International,* **2**, pp. 659–662 Vol.2.

[13] Carkhuff, B., and Cain, R., 2003. "Corrosion sensors for concrete bridges." *IEEE Instrumentation & Measurement Magazine,* **6**(2), June, pp. 19–24.

[14] Philipose, M., Smith, J. R., Jiang, B., Mamishev, A., Roy, S., and Sundara-Rajan, K., 2005. "Battery-free wireless identification and sensing." *IEEE Pervasive Computing,* **4**(1), pp. 37–45.

[15] Howell, L. L., 2001. *Compliant Mechanisms*. Wiley-Interscience.

[16] Jensen, B. D., 1998. "Identification of macro- and micro- compliant mechanism configurations resulting in bistable behavior." Master's thesis, Brigham Young University.

[17] Jensen, B., Howell, L. L., and Salmon, L. G., 1999. "Design of two-link, in-plane, bistable compliant micro-mechanism." *Journal of Mechanical Design,* **121**, pp. 417–423.

[18] Gomm, T., Howell, L. L., and Selfridge, R. H., 2002. "In-plane linear displacement bistable microrelay." *Journal of Micromechanics and Microengineering,* **12**, pp. 257–264.

[19] Jensen, B., Parkinson, M., Kurabayashi, K., Howell, L. L., and Baker, M. S., 2001. "Design optimization of a fully-compliant bistable micro-mechanism." *Proceedings of 2001 ASME International Mechanical Engineering Congress and Exposition*.

[20] Qiu, J., Lang, J., and Slocum, A., 2001. "A centrally-clamped parallel-beam bistable mems mechanism." *Micro Electro Mechanical Systems, 2001. MEMS 2001. The 14th IEEE International Conference on*, pp. 353–356.

[21] Singh, S. P., Burgess, G., and Singh, J., 2004. "Measurement and analysis of the second-day air small and light-weight package shipping environment within federal express." *Packaging Technology and Science,* **17**, pp. 119–127.

[22] Ostrem, F. E., and Godshall, W. D., 1979. An assesment of the common carrier shipping environment Tech. rep., U.S. Department of Agriculture.

[23] [Online].Available: http://www.shockwatch.com.

[24] Shepard, S., 2005. *RFID: Radio Frequency Identification*. McGraw Hill, New York.

[25] [Online].Available: http://www.asentrix.com.

[26] [Online].Available: http://www.trolleyscan.com.

[27] Hamrita, T. K., and Hoffacker, E. C., 2005. "Development of a "smart" wireless soil monitoring sensor prototype using RFID technology." *Applied Engineering in Agriculture,* **21**(1), pp. 139–143.

[28] Parkinson, M., Jensen, B., and Roach, G., 2000. "Optimization-based design of a fully-compliant bistable micromechanism." In *ASME 2000 Design Engineering Technical Conference*, no. DETC2000MECH-14119 in 2000.

[29] Hansen, B., Carron, C., Jensen, B., Hawkins, A., and Schultz, S., 2007. "Plastic latching accelerometer based on bistable compliant mechanisms." *Smart Materials and Structures,* **16**, pp. 1967–1972.

[30] Brinson, H. F., and Brinson, L. C., 2008. *Polymer Engineering Science and Viscoelasticity*. Springer Science+Business Media, LLC.

[31] Gerdeen, J. C., Lord, H. W., and Rorrer, R. A. L., 2006. *Engineering Design with Polymers and Composites*. CRC Press Taylor and Francis Group, LLC.

[32] Bicerano, J., 2002. *Prediction of Polymer Properties*. Marcel Dekker, Inc.

[33] Mortensen, C. R., Weight, B. L., Howell, L. L., and Magleby, S. P., 2000. "Compliant mechanism prototyping." In *Proc. ASME 2000 Design Engineering Technical Conferences*, no. DETC2000/MECH-14204.

[34] Robison, A., 2006. "Modeling and validation of tension element based mechanisms for golf ball-club impact." Master's thesis, Brigham Young University.

[35] Parise, J., Howell, L. L., and Magleby, S. P., 2001. "Ortho-planar linear-motion springs." *Mechanism and Machine Theory,* **36**(11-12), pp. 1281–1299.

[36] Soroushian, P., Chowdhury, H., and Nossoni, A., 2003. "Design and experimental verification of pseudoelastic-based constant-force springs." *Journal Of Intelligent Material Systems And Structures,* **14**(8), pp. 475–481.

[37] Vehar, C., Kota, S., and Dennis, R., 2004. "Closed-loop tape springs as fully compliant mechanisms - preliminary investigations." In *Proc. ASME 2004 Design Engineering Technical Conferences*, no. DETC2004-57403.

[38] Miller, S. F., Kao, C., Shih, A. J., and Qu, J., 2005. "Investigation of wire electrical discharge machining of thin cross-sections and compliant mechanisms." *International Journal of Machine Tools & Manufacture,* **45**(15), pp. 1717–1725.

[39] Cannon, J. R., and Howell, L. L., 2005. "A compliant contact-aided revolute joint." *Mechanism & Machine Theory,* **40**(11), pp. 1273–1293.

[40] Crane, N. B., Howell, L. L., Weight, B. L., and Magleby, S. P., 2004. "Compliant floating-opposing-arm (FOA) centrifugal clutch." *Journal of Mechanical Design,* **126**(1), pp. 169–177.

[41] Pendleton, T. M., and Jensen, B. D., 2007. "Compliant mechanisms formed from shaped wire." In *Proc. ASME 2007 Int. Des. Eng. Tech. Conf.*, no. DETC2007-34969.

[42] Todd, R. H., Allen, D. K., and Alting, L., 1994. *Manufacturing Processes Reference Guide*. Industrial Press Inc.

[43] Shoup, T. E., and McLarnan, C. W., 1971. "On the use of the undulating elastica for the analysis of flexible link mechanisms." *J. Engineering for Industry*, Feb., pp. 263–267.

[44] ASMI, 2002. *Atlas of Stress-Strain Curves*. American Society For Metals International.

[45] Cherry, B., 2008. "Characterizing the three-dimensional behavior of bistable micromechanisms." Master's thesis, Brigham Young University.

Appendix A

Ansys Batch File For Twisted Metal Rotation Points

```
!=========================================================
!Created by Ben Todd 2 Feb 08
!Compliant Bistable Mechanism, with butterfly compliant members.
!
!
!=========================================================
/TITLE,Twist Analysis of a rotation flexure for a FCBM
/CLEAR,NOSTART
/PREP7
PI=acos(-1)
!=========================================================
! INPUT PARAMETERS
!=========================================================
!/INPUT,paramfile,txt
a =    0.3778054272632
b =    0.7556108545264
ww =    1.1334162817895
l =    2.500000000000
ll =    20.0000000000000
t =    0.1016
theta =    2*Pi/180
fillet = .2032
tr= t
L1 = l
h1 = .3 !width of thin flexure
theta1 = theta
L2 = l
h2 = .3 !width of thin flexure
theta2 = theta
Lr = ll
hr = 2.7 !width of thick flexure
thetar = theta

swidth=4
```

```
sheight=8
Ey = 201111.111 !200000
Pr = .30
NLegs=2
dY = 90*Pi/180
/NOPR

ET,1,SOLID95

MP,EX,1,Ey !*** Youngs Modulus ***
MP,EY,1,Ey !*** Youngs Modulus ***
MP,EZ,1,Ey !*** Youngs Modulus ***

MP,PRXY,1,Pr !*** Poisson's Ratio ***
MP,PRYZ,1,Pr !*** Poisson's Ratio ***
MP,PRXZ,1,Pr !*** Poisson's Ratio ***

!Set's up stress Strain curve desired.
TB,MELA,1,1,13,
TBTEMP,0
TBPT,,0,0
TBPT,,.0036,724
TBPT,,.004,765
TBPT,,.005,792
TBPT,,.0075,820
TBPT,,.01,896
TBPT,,.02,1075
TBPT,,.03,1200
TBPT,,.04,1282
TBPT,,.05,1337
TBPT,,.06,1365
TBPT,,.0625,1372

Nonlinear = 1
Steps = 10 !10

!=========================================================
! MODEL SETUP
!=========================================================
K,3,0,0,0

K,4,h1/2*sin(theta1),h1/2*cos(theta1),0
K,5,-h1/2*sin(theta1),-h1/2*cos(theta1),0

K,8,-h1/2*sin(theta1)+L1,h1/2*cos(theta1),0
```

```
K,9,h1/2*sin(theta1)+L1,-h1/2*cos(theta1),0

K,10,-h1/2*sin(theta1)+L1,hR/2,0
K,11,h1/2*sin(theta1)+L1,-hR/2,0

K,12,-h1/2*sin(theta1)+L1+Lr,hR/2,0
K,13,h1/2*sin(theta1)+L1+Lr,-hR/2,0

K,14,-h1/2*sin(theta1)+L1+Lr,h1/2*cos(theta1),0
K,15,h1/2*sin(theta1)+L1+Lr,-h1/2*cos(theta1),0

K,16,-h1/2*sin(theta1)+L1+Lr+L2,h1/2*cos(theta1),0
K,17,h1/2*sin(theta1)+L1+Lr+L2,-h1/2*cos(theta1),0


K,18,-h1/2*sin(theta1)+L1+Lr+L2+sheight/2*sin(theta1),
sheight/2*cos(theta1),0
K,19,h1/2*sin(theta1)+L1+Lr+L2-sheight/2*sin(theta1),
-sheight/2*cos(theta1),0


K,20,-h1/2*sin(theta1)+L1+Lr+L2+sheight/2*sin(theta1)+swidth,
sheight/2*cos(theta1),0
K,21,h1/2*sin(theta1)+L1+Lr+L2-sheight/2*sin(theta1)+swidth,
-sheight/2*cos(theta1),0

K,22,sheight/2*sin(theta1),sheight/2*cos(theta1),0
K,23,-sheight/2*sin(theta1),-sheight/2*cos(theta1),0

K,24,sheight/2*sin(theta1)-swidth,sheight/2*cos(theta1),0
K,25,-sheight/2*sin(theta1)-swidth,-sheight/2*cos(theta1),0

K,26,-sheight/2*sin(theta1)-swidth,-sheight/2*cos(theta1),t

!bottom plane
L,4,8
L,8,10
L,10,12
L,12,14
L,14,16
L,16,18
L,18,20
L,20,21
L,21,19
L,19,17
```

```
L,17,15
L,15,13
L,13,11
L,11,9
L,9,5
L,5,23
L,23,25
L,25,24
L,24,22
L,22,4



LFILLT,1,2,fillet
LFILLT,4,5,fillet
LFILLT,5,6,fillet
LFILLT,10,11,fillet
LFILLT,11,12,fillet
LFILLT,14,15,fillet
LFILLT,15,16,fillet
LFILLT,20,1,fillet
AL,ALL

!***Creates volume****
L,25,26
VDRAG,1,,,,,,29


!*** MESH MECHANISMS ***

MSHAPE,1,3D
ESIZE,0.25
ALLSEL,ALL
VMESH,ALL
VIMP,ALL,1,3


! SELECT THE AREAS ASSOCIATED WITH THE FILLETS
ASEL,S,AREA,,21,23,1
ASEL,A,AREA,,2,3,1
ASEL,A,AREA,,29
ASEL,A,AREA,,7,9,1
ASEL,A,AREA,,15,17,1
```

```
! SELECT THE NODES ASSOCIATED WITH THE AREAS
NSLA,S,1


! REFINE THE ELEMENTS ARROUND THE SELECTED ELEMENTS

NREFINE,ALL,,,1,1,CLEAN

! SELECT THE ELEMENTS ASSOCIATED WITH THOSE AREAS

ALLSEL,ALL

VIMP,ALL,1,3


!=========== Structural Boundary Constraints ===========

! CONSTRAIN THE RIGHT SIDE OF THE DEVICE

ASEL,S,AREA,,12
NSLA,S,1
!D,ALL,UX,0 !Right End
D,ALL,UZ,0 !Right End

ASEL,S,AREA,,11,13,2
NSLA,S,1
D,ALL,UZ,0
ALLSEL,ALL


! CONSTRAIN THE LEFT SIDE OF THE DEVICE IN ALL DOF
ASEL,S,AREA,,25,27,1
NSLA,S,1
D,ALL,ALL

ALLSEL,ALL



FINISH
!=========================================================
! SOLUTION STEPS
!=========================================================
/SOLU
NLGEOM,1 !***Nonlinear Analysis****
```

```
ANTYPE,0 !***Static Analysis Type***
!============ ROTATIONAL DISPLACEMENT =============
*DO,mm,1,Steps+1,1
ASEL,S,AREA,,5
NSLA,S,1
NSEL,R,LOC,Z,T/2

D,ALL,UZ,-hr/2*sin((mm-1)*dY/Steps)
D,ALL,UY,-(hr/2-hr/2*cos((mm-1)*dY/Steps))

ALLSEL,ALL

ASEL,S,AREA,,19
NSLA,S,1
NSEL,R,LOC,Z,T/2

D,ALL,UZ,hr/2*sin((mm-1)*dY/Steps)
D,ALL,UY,(hr/2-hr/2*cos((mm-1)*dY/Steps))

ALLSEL,ALL

lswrite,mm
*ENDDO
lssolve,1,Steps+1
FINISH
/POST1
```

Appendix B

Elliptic Integral Model .M Files

```
%findalphanewn.m - This function finds alpha, the nondimensionalized
%force, for motion of the end of a guided beam along a line with
%angle gamma from the vertical.
clear all
t = .7;%mm
l = 25;%mm
gamma = 6;%degrees


slen = t^2/(12*l^2);%0.00083333;
bmax = 1.6*tand(gamma);
numbs = 100;
b = [bmax/numbs:bmax/numbs:bmax];
%b = b(1:end-5);
a = 1-b*tand(gamma);
guess = [0 0.05];
%guess2 = [0 0.05];
%guess3 = [0 0.05];

for counter = 1:length(b)

    [n(counter),k1,alpha(counter),aout(counter),bout(counter),...
    isgood(counter),aerr(counter),berr(counter),sigma(counter),...
    x(:,counter),y(:,counter)] = findabnewn(a(counter),...
    b(counter),2,slen,guess);
    mode(counter) = 2;
    if isgood(counter)~=1
            [n(counter),k1,alpha(counter),aout(counter),...
            bout(counter),isgood(counter),aerr(counter),...
            berr(counter),sigma(counter),x(:,counter),y(:,counter)] =
            findabnewn(a(counter),b(counter),1,slen,guess);
            mode(counter) = 1;
    end
    %[n3(counter),k3,alpha3(counter),aout3(counter),bout3(counter),...
```

```
    isgood3(counter),aerr3(counter),berr3(counter),sigma3(counter),...
    x3(:,counter),y3(:,counter)] = findabnewn(a(counter),...
    -b(counter),3,slen,guess3);
    counter
    guess = [n(counter) k1];
    %guess2 = [n2(counter) k2];
%     if isgood3(counter)==1
%         guess3 = [n3(counter) k3];
%     end
end


figure(1)
clf
plot(aout,bout,'o',a,b)
% hold on
% plot([aout2],[bout2],'rs')
%plot(aout3,-bout3,'g*')
xlabel('Horizontal Motion')
ylabel('Vertical Motion')

% bad = find(isgood==0);
% bad2 = find(isgood2==0);
%bad3 = find(isgood3==0);



% alpha(bad) = NaN;
% alpha2(bad2) = NaN;
% %alpha3(bad3) = NaN;
%
% aerr(bad) = NaN;
% aerr2(bad) = NaN;
% %aerr3(bad) = NaN;
%
% berr(bad) = NaN;
% berr2(bad) = NaN;
%berr3(bad) = NaN;


alphafsq = alpha.^2.*(n.*cosd(gamma) + sind(gamma));
%alphafsq2 = alpha2.^2.*(n2.*cosd(gamma) + sind(gamma));
%alphafsq3 = alpha3.^2.*(-n3.*cosd(gamma) + sind(gamma));
```

```
del = sqrt((1-a).^2+b.^2);
figure(4)
clf
plot(del,alphafsq)
hold on
%plot(del,alphafsq2,'r')
%plot(del,alphafsq3,'g')
xlabel('Normalized Displacement')
ylabel('Normalized Force')

maxaerr = max(aerr)
%maxaerr2 = max(aerr2)
%maxaerr3 = max(aerr3)

maxberr = max(berr)
%maxberr2 = max(berr2)
%maxberr3 = max(berr3)

err1 = sqrt((aout-a).^2 + (bout - b).^2);
%err2 = sqrt((aout2 - a).^2 + (bout2 - b).^2);
%use2 = find(err2<err1);
nt = n;
%nt(use2) = n2(use2);
alphat = alpha;
%alphat(use2) = alpha2(use2);
alphaft = alphafsq;
%alphaft(use2) = alphafsq2(use2);
sigmat = sigma;
%sigmat(use2) = sigma2(use2);
equilib = find((alphaft(1:end-1).*alphaft(2:end))<0);
psi = cumtrapz([0 del],[0 alphaft]);
if isempty(equilib)
    display('Not Bistable')
else
    stable = equilib(2);
    unstable = equilib(1);
    dels = del(stable) - alphaft(stable)*(del(stable+1) - ...
    del(stable))/(alphaft(stable+1) - alphaft(stable));
    psis = psi(stable+1) + (psi(stable+2)-psi(stable+1))*...
    (dels - del(stable))/(del(stable+1) - del(stable));
    maxs = max(sigmat(1:stable))
    stablepos = dels*l
    delu = del(unstable) - alphaft(unstable)*(del(unstable+1) -...
    del(unstable))/(alphaft(unstable+1) - alphaft(unstable));
    unstablepos = delu*l
```

```
end

figure(2)
clf
plot(del,nt)
xlabel('Normalized Displacement')
ylabel('n')
figure(3)
plot(del,alphat)
xlabel('Normalized Displacement')
ylabel('Normalized Horizontal Force')
figure(5)
clf
plot(del,alphaft)
xlabel('Normalized Displacement')
ylabel('Normalized Force Along Line of Displacement')
figure(6)
clf
plot(del,sigmat);
xlabel('Normalized Displacement')
ylabel('Normalized Stress')
figure(7)
clf
plot([0 del],psi)
xlabel('Normalized Displacement')
ylabel('Normalized Energy')

xt = x;
%xt(:,use2) = x2(:,use2);
yt = y;
%yt(:,use2) = y2(:,use2);
figure(8)
clf
plot(xt,yt)
title('Deflected Beam Shapes')

function [n,k,alpha,aout,bout,isgood,aerr,berr,sigma,x,y] =...
findabnewn(a,b,mode,slen,guess)
tol = 1e-4;
options = optimset('TolFun',1e-9,'MaxFunEvals',10000);
outvals = fsolve(@solvefn,guess,options,a,b,mode,slen);
[as,bs,alpha,s,theta,x,y,beta] =...
 guidednonlin(outvals(2),outvals(1),mode);
n = outvals(1)
k = outvals(2);
```

```
if x==0
    aout = as;
    bout = bs;
    aerr = 0;
    berr = 0;
    sigma = 0;
else
%     dxi = ones(size(x));
%     dyi = zeros(size(y));
%     dxi(2:end-1,:) = (x(3:end,:) -...
 x(2:end-1,:))./(2*(s(3:end,:) - s(2:end-1,:))) + ...
%         (x(2:end-1,:) - x(1:end-2,:))./(2*(s(2:end-1,:) -...
 s(1:end-2,:)));
%     dyi(2:end-1,:) = (y(3:end,:) -...
 y(2:end-1,:))./(2*(s(3:end,:) - s(2:end-1,:))) + ...
%         (y(2:end-1,:) - y(1:end-2,:))./(2*(s(2:end-1,:) -...
 s(1:end-2,:)));
%
%     theta = atan2(dyi,dxi);
    sigma = max(slen*alpha.^2.*(cos(theta) - n*sin(theta)) +...
    sqrt(12*slen)*beta/2);
    sa = (cos(theta)).^2 - n*sin(theta).*cos(theta);
    sb = cos(theta).*sin(theta) - n*(sin(theta)).^2;
    isa = (sa(1:end-1,:) + sa(2:end,:)).*(s(2:end,:) -...
     s(1:end-1,:))/2;
    isb = (sb(1:end-1,:) + sb(2:end,:)).*(s(2:end,:) -...
     s(1:end-1,:))/2;
    da = slen*alpha.^2.*sum(isa,1);
    db = slen*alpha.^2.*sum(isb,1);
    aerr = da./as;
    berr = db./bs;
    aout = as - da;
    bout = bs - db;
end
pererr = abs((aout - a)/(1-a));
pererrb = abs((bout - b)/b);
if pererr>tol | pererrb>tol
    %outvals = fsolve(@solvefn,[100 .1],options,a,b,mode,slen);
%     [aout,bout,alpha] =...
 guidednonlin(outvals(2),outvals(1),mode);
%     n = outvals(1)
%     k = outvals(2);
%     pererr = abs((aout*(1 - n*(alpha.^2)*slen) - a)/a);
%     pererrb = abs((bout*(1-n*(alpha.^2)*slen) - b)/b);
%     if pererr>tol | pererrb>tol
```

```
        isgood = 0;
%     else
%         isgood = 1;
%     end
else
    isgood = 1;
end

function about = solvefn(x,ain,bin,mode,slen)
n = x(1);
k = x(2);
eta = sqrt(1+n.^2);
kmin = sqrt((eta - 1)/(2*eta));
if k<=kmin
    newa = 1+(kmin-k);
    newb = 0-(kmin-k);
elseif k>=1
    newa = 1+(k-1);
    newb = -(k-1);
else
    [a,b,alpha,s,theta] = guidednonlin(k,n,mode);
%     dxi = ones(size(x));
%     dyi = zeros(size(y));
%     dxi(2:end-1,:) = (x(3:end,:) -...
 x(2:end-1,:))./(2*(s(3:end,:) - s(2:end-1,:))) + ...
%         (x(2:end-1,:) - x(1:end-2,:))./(2*(s(2:end-1,:) -...
 s(1:end-2,:)));
%     dyi(2:end-1,:) = (y(3:end,:) -...
 y(2:end-1,:))./(2*(s(3:end,:) - s(2:end-1,:))) + ...
%         (y(2:end-1,:) - y(1:end-2,:))./(2*(s(2:end-1,:) -...
 s(1:end-2,:)));
%
%     theta = atan2(dyi,dxi);
    sa = (cos(theta)).^2 - n*sin(theta).*cos(theta);
    sb = cos(theta).*sin(theta) - n*(sin(theta)).^2;
    isa = (sa(1:end-1,:) + sa(2:end,:)).*(s(2:end,:) -...
     s(1:end-1,:))/2;
    isb = (sb(1:end-1,:) + sb(2:end,:)).*(s(2:end,:) -...
     s(1:end-1,:))/2;
    da = slen*alpha.^2.*sum(isa,1);
    db = slen*alpha.^2.*sum(isb,1);
    newa = a - da;
    newb = b - db;
end
about(1) = (ain - newa);
```

```
about(2) = (bin - newb);


function [a,b,alpha,s,theta,x,y,beta] = guidednonlin(k,n,mode)
%This function calculates end coordinates and loads for a beam.
%Inputs are k, the elliptic integral modulus, and n, the ratio
%of the transverse force to the axial compressive force. Either
%may be a row vector. If both are vectors, they must be the same
%length.
%Outputs are a, the nondimensional horizontal displacement, b, the
%nondimensional vertical displacment, and alpha, the
%nondimensional load.
%beta1 and beta2 are the nondimensional moment at the fixed and
%guided beam
%ends, respectively.
%Additionally, outputs x and y give the beam shape.
%Assumptions are an initially-straight guided beam with end loads
%and moments.

eta = sqrt(1+n.^2);
kmin = sqrt((eta - 1)/(2*eta));
if k<=kmin
    a = 1+10*(kmin-k);
    b = 0-10*(kmin-k);
    alpha = 0;
    x = zeros(101,1);
    y = x;
    s = x;
    beta = x;
    theta = x;
    return
elseif k>=1
    a = 1+10*(k-1);
    b = -10*(k-1);
    alpha = 0;
    x = zeros(101,1);
    y = x;
    s = x;
    beta = x;
    theta = x;
    return
end
if n>=0
phi1 = asin(sqrt((eta - 1)./(2*eta.*k.^2)));
else
```

```
    phi1 = -asin(sqrt((eta - 1)./(2*eta.*k.^2)));
end
switch mode
    case 1
        phi2 = pi - phi1;%first mode
    case 2
        phi2 = 2*pi+phi1;%second mode
    case 3
        phi2 = 3*pi - phi1;%third mode
    case 4
        phi2 = 4*pi+phi1;%fourth mode
    case 5
        phi2 = 5*pi - phi1;%fifth mode
    case 6
        phi2 = 6*pi + phi1;%sixth mode
    case 7
        phi2 = 7*pi - phi1;%seventh mode
    case 8
        phi2 = 8*pi + phi1;%eigth mode
    case 9 %third mode, second type
        phi = asin(sqrt((eta - 1)./(2*eta.*k.^2)));
        if n>=0
            phi1 = pi-phi;
            phi2 = 4*pi + phi;
        else
            phi1 = pi + phi;
            phi2 = 4*pi - phi;
        end
end
[f1,e1] = elliptic12(phi1,k.^2);
[f2,e2] = elliptic12(phi2,k.^2);
alpha = (f2 - f1)./sqrt(eta);
a = ((f1 - f2 + 2*(e2 - e1)) - ...
    2*n.*k.*(cos(phi2) - cos(phi1)))./(alpha.*(eta.^(3/2)));
b = (n.*(f2 - f1 + 2*(e1 - e2)) + ...
    2*k.*(cos(phi1)-cos(phi2)))./(alpha.*(eta.^(3/2)));
[x,y,s,beta,theta] =...
 guidedbeamshape(n,eta,phi1,phi2,k,alpha,f1,e1);


function [x,y,s,beta,theta] =...
 guidedbeamshape(n,eta,phi1,phi2,k,alpha,f1,e1);

if size(phi1,1)>1
    n = n';
```

```
    eta = eta';
    phi1 = phi1';
    phi2 = phi2';
    k = k';
    alpha = alpha';
    f1 = f1';
    e1 = e1';
end

numpts = 100;
phi = zeros(numpts+1,length(phi1));
for counter = 1:length(phi1)
phi(:,counter) = [phi1(counter):(phi2(counter) -...
phi1(counter))/numpts:phi2(counter)]';
end
temp2 = ones(size(phi,1),1);
if length(n)==1
    n = n*ones(size(phi1));
    eta = eta*ones(size(phi1));
end
[f2,e2] = elliptic12(phi,temp2*(k.^2));
x = ((2*(e2 - temp2*e1)-f2 + temp2*f1) ...
    - 2*(temp2*n).*(temp2*k).*(cos(phi) -...
     cos(temp2*phi1))).//((temp2*alpha).*(temp2*(eta.^(3/2))));
y = (-(temp2*n).*(2*(e2 - temp2*e1)-f2 + temp2*f1) - ...
    2*(temp2*k).*(cos(phi) -...
    cos(temp2*phi1))).//((temp2*alpha).*(temp2*(eta.^(3/2))));
s = (f2 - temp2*f1).//((temp2*alpha).*(temp2*sqrt(eta)));
beta = 2*(temp2*k).*(temp2*alpha).*sqrt(temp2*eta).*cos(phi);
theta = 2*(asin((temp2*k).*sin(phi))-...
asin((temp2*k).*sin(temp2*phi1)));

function [F,E,Z] = elliptic12(u,m,tol)
% ELLIPTIC12 evaluates the value of the Incomplete Elliptic
%Integrals of the First, Second Kind and Jacobi's Zeta Function.
%
%   [F,E,Z] = ELLIPTIC12(U,M,TOL) where U is a phase in radians,
% 0<M<1 is the module and TOL is the tolerance (optional).
%Default value for
%   the tolerance is eps = 2.220e-16.
%
%   ELLIPTIC12 uses the method of the Arithmetic-Geometric Mean
%   and Descending Landen Transformation described in [1] Ch.
%   17.6, to determine the value of the Incomplete Elliptic
%   Integrals of the First, Second Kind and Jacobi's Zeta
```

```
%   Function [1], [2].
%
%       F(phi,m) = int(1/sqrt(1-m*sin(t)^2), t=0..phi);
%       E(phi,m) = int(sqrt(1-m*sin(t)^2), t=0..phi);
%       Z(phi,m) = E(u,m) - E(m)/K(m)*F(phi,m).
%
%   Tables generating code ([1], pp. 613-621):
%   [phi,alpha] = meshgrid(0:5:90, 0:2:90);
%   modulus and phase in degrees
%   [F,E,Z] = elliptic12(pi/180*phi, sin(pi/180*alpha).^2);
%   values of integrals
%
%   See also ELLIPKE, ELLIPJ, ELLIPTIC3, THETA, AGM.
%
%   References:
%   [1] M. Abramowitz and I.A. Stegun, "Handbook of Mathematical
%   Functions", Dover Publications", 1965, Ch. 17.1 - 17.6(by L.M.
%   Milne-Thomson).
%   [2] D. F. Lawden, "Elliptic Functions and Applications"
%       Springer-Verlag, vol. 80, 1989

%   For support, please reply to
%       moiseev[at]sissa.it, moiseev.igor[at]gmail.com
%       Moiseev Igor,
%       34106, SISSA, via Beirut n. 2-4,  Trieste, Italy
%
%   The code is optimized for ordered inputs produced by the
%   functions meshgrid, ndgrid. To obtain maximum performace (up
%   to 30%) for singleton,
%   1-dimensional and random arrays remark call of the function
%   unique(.) and edit further code.

if nargin<3, tol = eps; end
if nargin<2, error('Not enough input arguments.'); end

if ~isreal(u) || ~isreal(m)
    error('Input arguments must be real.')
end

if length(m)==1, m = m(ones(size(u))); end
if length(u)==1, u = u(ones(size(m))); end
if ~isequal(size(m),size(u)), error('U and M must be the same...
 size.'); end

F = zeros(size(u));
```

```
E = F;
Z = E;
m = m(:).';    % make a row vector
u = u(:).';

if any(m < 0) || any(m > 1), error('M must be in the range ...
0 <= M <= 1.'); end

I = uint32( find(m ~= 1 & m ~= 0) );
if ~isempty(I)
    [mu,J,K] = unique(m(I));   % extracts unique values from m
    K = uint32(K);
    mumax = length(mu);
    signU = sign(u(I));

    % pre-allocate space and augment if needed
chunk = 7;
a = zeros(chunk,mumax);
c = a;
b = a;
a(1,:) = ones(1,mumax);
c(1,:) = sqrt(mu);
b(1,:) = sqrt(1-mu);
n = uint32( zeros(1,mumax) );
i = 1;
while any(abs(c(i,:)) > tol)    % Arithmetic-Geometric Mean ...
of A, B and C
        i = i + 1;
        if i > size(a,1)
          a = [a; zeros(2,mumax)];
          b = [b; zeros(2,mumax)];
          c = [c; zeros(2,mumax)];
        end
        a(i,:) = 0.5 * (a(i-1,:) + b(i-1,:));
        b(i,:) = sqrt(a(i-1,:) .* b(i-1,:));
        c(i,:) = 0.5 * (a(i-1,:) - b(i-1,:));
        in = uint32( find((abs(c(i,:)) <= tol) & (abs(c(i-1,:))...
         > tol)) );
        if ~isempty(in)
          [mi,ni] = size(in);
          n(in) = ones(mi,ni)*(i-1);
        end
end

    mmax = length(I);
```

```
mn = double(max(n));
phin = zeros(1,mmax);     C  = zeros(1,mmax);
Cp = C;  e  = uint32(C);  phin(:) = signU.*u(I);
i = 0;   c2 = c.^2;
while i < mn            % Descending Landen Transformation
        i = i + 1;
        in = uint32(find(n(K) > i));
        if ~isempty(in)
            phin(in) =...
             atan(b(i,K(in))./a(i,K(in)).*tan(phin(in))) + ...
                pi.*ceil(phin(in)/pi - 0.5) + phin(in);
            e(in) = 2.^(i-1) ;
            C(in) = C(in)  + double(e(in(1)))*c2(i,K(in));
            Cp(in)= Cp(in) + c(i+1,K(in)).*sin(phin(in));
        end
end

    Ff = phin ./ (a(mn,K).*double(e)*2);
    F(I) = Ff.*signU;     % Incomplete Ell. Int. of the First Kind
    Z(I) = Cp.*signU;     % Jacobi Zeta Function
    E(I) = (Cp + (1 - 1/2*C) .* Ff).*signU;
    % Incomplete Ell. Int. of the Second Kind
end

% Special cases: m == {0, 1}
m0 = find(m == 0);
if ~isempty(m0), F(m0) = u(m0); E(m0) = u(m0); Z(m0) = 0; end

m1 = find(m == 1);
um1 = abs(u(m1));
if ~isempty(m1),
    N = floor( (um1+pi/2)/pi );
    M = find(um1 < pi/2);

    F(m1(M)) = log(tan(pi/4 + u(m1(M))/2));
    F(m1(um1 >= pi/2)) = Inf.*sign(u(m1(um1 >= pi/2)));

    E(m1) = ((-1).^N .* sin(um1) + 2*N).*sign(u(m1));

    Z(m1) = (-1).^N .* sin(u(m1));
end
```